International Journal of Greenhouse Gas Control 93 (2020) 102898

Contents lists available at ScienceDirect

International Journal of Greenhouse Gas Control

journal homepage: www.elsevier.com/locate/ijggc

Development of tailor-made oxygen carriers and reactors for chemical looping processes at Huazhong University of Science & Technology

Haibo Zhao[a,*], Xin Tian[a], Jinchen Ma[a], Mingze Su[a], Baowen Wang[b], Daofeng Mei[c]

[a] State Key Laboratory of Coal Combustion, School of Energy and Power Engineering, Huazhong University of Science and Technology, Wuhan 430074, PR China
[b] College of Electric Power, North China University of Water Resources and Electric Power, Zhengzhou 450045, PR China
[c] College of Engineering, Huazhong Agricultural University, Wuhan 430070, PR China

ARTICLE INFO

Keywords:
Carbon capture
Chemical looping
Tailor-made oxygen carrier
Inter-connected fluidized bed reactor
Reaction kinetics
Density functional theory

ABSTRACT

For the concerns of global warming, there is an urgent need of green, low-cost, and sustainable ways for the conversion and utilization of fossil energy. Holding the merit of inherent CO_2 separation during carbonaceous fuel conversion, chemical looping technique is emerging as a perfect alternative to conventional fossil fuel conversion processes. Central to this technique is the design of high-performance oxygen carriers and suitable reactors that can efficiently realize the cyclic redox loop involved. To date, plenty kinds of (over 1200) oxygen carriers have been screened, synthesized and investigated by different research groups worldwide. Dozens of chemical looping reactors with thermal power ranged from kW_{th} to MW_{th} were also constructed and successfully operated. All these help to support the commercial demonstration and even industrial application of this innovative fuel conversion and carbon capture technique.

The chemical looping related research at Huazhong University of Science & Technology (HUST) has experienced rapid development during the past 10 years, from rational synthesis of oxygen carrier to inter-connected fluidized bed reactor design and operation. In this article, the development of tailor-made oxygen carriers and active design of reactors at HUST is comprehensively reviewed and appraised, including the screening and optimization of oxygen carriers, reduction kinetics of oxygen carriers with gaseous fuels, microcosmic level understanding of the reaction mechanism in chemical looping *via* density functional theory (DFT) calculation, rational design and controllable synthesis of a hierarchically-structured oxygen carrier, and negative effects of pollutants (like sulfur and chlorides) on oxygen carriers. Moreover, experience gained from the design, macro simulation and modeling as well as continuous operation of inter-connected fluidized bed reactors is also provided. Overall, more than 100 different oxygen carriers based on Fe-, Cu-, Mn-, Ni-, as well as mixed oxides and natural ores, are systematically reviewed in terms of different chemical looping processes. The rational design route of a representative $CuO@TiO_2$-Al_2O_3 oxygen carrier is proposed from the bottom up, on the basis of DFT calculation, molecular dynamic (MD) simulation, and detailed kinetics analysis. Over 300 h of continuous operation experience of the inter-connected fluidized bed reactor contributes to the demonstration of this technique. Numerical simulation *via* commercial computational fluid dynamics (CFD) software further helped the design, optimization, and scale-up of the reactor. In general, this review paper outlines the research route of chemical looping at HUST in details, which is expected to provide useful reference and guidance for the relevant readers.

1. Introduction

With the growing demand of greener ways for fossil fuel conversion, chemical looping techniques have been gaining increasing interests around the world as an efficient way to generate clean energy and/or value-added chemicals with near-zero carbon emission. (Adanez et al., 2012; Adánez et al., 2018) The basic principle behind chemical looping is utilizing a kind of solid intermediate to transfer energy and substances, splitting one reaction into two or more sub-reactions *via* isolated steps or divided spaces, so as to achieve *in situ* separation of the desired products. During the past three decades, chemical looping processes have witnessed an extensive development in techniques including chemical looping full oxidation (*i.e.*, chemical looping combustion, CLC (Abad et al., 2015a; Bao et al., 2014a, b; Gu et al., 2015;

* Corresponding author.
E-mail address: hzhao@mail.hust.edu.cn (H. Zhao).

https://doi.org/10.1016/j.ijggc.2019.102898
Received 18 July 2019; Received in revised form 31 October 2019; Accepted 4 November 2019
Available online 22 November 2019
1750-5836/

Hossain and de Lasa, 2008; Ishida and Jin, 1994; Lyngfelt, 2014); *in situ* gasification chemical looping combustion, *i*G-CLC (Abad et al., 2018; Mendiara et al., 2012; Pérez-Vega et al., 2017); chemical looping with oxygen uncoupling, CLOU (Abad et al., 2012a; Imtiaz et al., 2013; Mattisson et al., 2009b)), chemical looping partial oxidation (also known as chemical looping reforming, CLR) (Lu et al., 2018; Neal et al., 2014; Ortiz et al., 2012; Tang et al., 2015; Zheng et al., 2017), chemical looping air separation (CLAS) (Moghtaderi, 2009; Shah et al., 2012; Wang et al., 2016d), chemical looping CO_2/H_2O splitting (He and Li, 2015; He et al., 2014; Ma et al., 2018c; Sun et al., 2019; Zhang et al., 2017; Zhu et al., 2018b), and chemical looping selective oxidation (Dudek et al., 2019; Neal et al., 2016; Tian et al., 2019; Yusuf et al., 2017). Despite the varied desirable products of the aforementioned chemical looping processes, they all involve the use of an oxygen carrier (Me_xO_y) to supply lattice (or gaseous) oxygen instead of air.

Chemical looping technique is not limited to oxidation reactions (Zeng et al., 2018), and if one replaces the oxygen carrier with CO_2 carrier, nitrogen carrier or even sulfur carrier, a broad application, like calcium looping (Qin et al., 2016; Sun et al., 2012), chemical looping ammonia synthesis (Michalsky et al., 2015), and chemical looping desulfurization (Brunet et al., 2005), can be achieved. Note that, all these chemical looping processes require atmosphere-isolated but interrelated sub-reactions to complete the transfer of energy and substances, which can be achieved by particle circulation based inter-connected reactors (Abad et al., 2015b; Bayham et al., 2013; Berguerand and Lyngfelt, 2008b; Ge et al., 2016; Ströhle et al., 2014), reaction atmosphere switching based single/multiple paralleled reactors (Jin and Ishida, 2002; Solunke and Veser, 2010; Wang et al., 2016d), or reactor switching based rotating reactor. (Håkonsen and Blom, 2011; Håkonsen et al., 2014; Zhao et al., 2012a, b)

For the case of a typical CLC process, the used oxygen carriers are usually transition metal oxides that are capable of withstanding repeated reduction and oxidation reactions under a cyclic redox scheme (Adánez et al., 2004; Mattisson, 2013) In CLC, the first step is the reduction of the oxygen carrier with fuel in the fuel reactor (FR), which generates a stream of CO_2 and H_2O. The reduced oxygen carrier is then transferred back to the air reactor (AR) to recuperate its oxygen carrying capacity by air oxidization, together with heat released to drive a steam turbine for power generation. (Tong et al., 2014) As fuel is converted in an air-free environment, there is no N_2 dilution of the combustion products. (Ishida and Jin, 1996) Therefore, high-purity CO_2 stream can be easily obtained after steam condensation of FR exhaust, without the need of energy-intensive gas-gas separation process. (Lyngfelt et al., 2001) Fig. 1 depicts a schematic view of the CLC process, as well as the key reactions occur therein.

For solid fuel like coal, as the solid-solid contact between oxygen carrier and coal was not favorable for fuel conversion in the fluidized-bed reactor, the coal conversion rate and combustion efficiency were thus limited to a certain extent. To resolve this issue, steam or CO_2 was introduced as char gasification agent in the FR, running under the so-called *i*G-CLC mode. Moreover, carbon stripper was configured to further convert of the escaped char residue from FR.

For the coal-derived *i*G-CLC process, reactions in the FR can be described as:

$$\text{Coal} \rightarrow \text{Char} + \text{Volatiles} \quad \text{(R1)}$$

$$\text{Char} + H_2O/CO_2 \rightarrow CO + H_2 + \text{Ash} \quad \text{(R2)}$$

$$Me_xO_y + CO, H_2, \text{Volatiles} \rightarrow Me_xO_{y-1} + CO_2 + H_2O \quad \text{(R3)}$$

While in the AR, the reduced oxygen carrier regenerates itself by O_2 (air) oxidation as:

$$Me_xO_{y-1} + 1/2O_2 \rightarrow Me_xO_y \quad \text{(R4)}$$

In order to overcome the low char gasification rate in the *i*G-CLC process, an alternative process was proposed by Mattisson et al. (2009b) for the conversion of solid fuels, known as chemical looping with oxygen uncoupling (CLOU). In CLOU, the oxygen carrier used should have the capability of releasing gaseous O_2 under certain conditions of high temperature and suitable equilibrium O_2 partial pressure. Therefore, the solid fuel can be directly converted by molecular oxygen *via* combustion reactions in CLOU, so as to attain much faster char conversion rate. (Mattisson et al., 2009a) The key step in CLOU is the thermal decoupling of oxygen carrier, generating gaseous O_2:

$$Me_xO_y \rightarrow Me_xO_{y-1} + 1/2O_2 \quad \text{(R5)}$$

Simultaneously, solid fuel undergoes devolatilization process at high temperature to produce volatile matters and residual char,

$$\text{Solid fuel} \rightarrow \text{Char} + \text{Volatiles} \quad \text{(R6)}$$

The volatile matters and char will be further converted by gaseous O_2, like in traditional fuel combustion processes,

$$\text{Char} + O_2 \rightarrow CO_2 + \text{ash} \quad \text{(R7)}$$

$$\text{Volatiles} + O_2 \rightarrow CO_2 + H_2O \quad \text{(R8)}$$

As can be anticipated, for the successful demonstration of chemical looping processes, there are two key issues to be addressed. One is the appropriate oxygen carrier, which should meet most of, if not all the criteria (will be discussed in Section 2.1) required under the rigorous cyclic redox process. The other is the suitable reactor. For the interconnected fluidized bed reactor, as adopted by HUST and widely investigated by many other groups (Cuadrat et al., 2011; Markström et al., 2014; Shen et al., 2009b; Ströhle et al., 2015), smooth solid circulation within the whole system is pivotal to realize the cyclic redox of oxygen carrier. The characteristics of different oxygen carriers should be crucial to their activity in chemical looping, *via* chemical reaction thermodynamics and physicochemical properties. While different configurations of the reactor would certainly exert significant impact on the overall performance of the whole reaction system.

This paper presents a comprehensive review on tailor-made oxygen carriers and reactors for chemical looping processes developed at Huazhong University of Science & Technology (HUST). For the review on oxygen carriers, emphasis will be laid on the application of different oxygen carriers to various chemical looping processes. The rational synthesis route of a typical Cu-based oxygen carrier ($CuO@TiO_2$-Al_2O_3) will be introduced in details. The reaction kinetics related to oxygen carriers as well as the negative effects of pollutants (like S and Cl) will

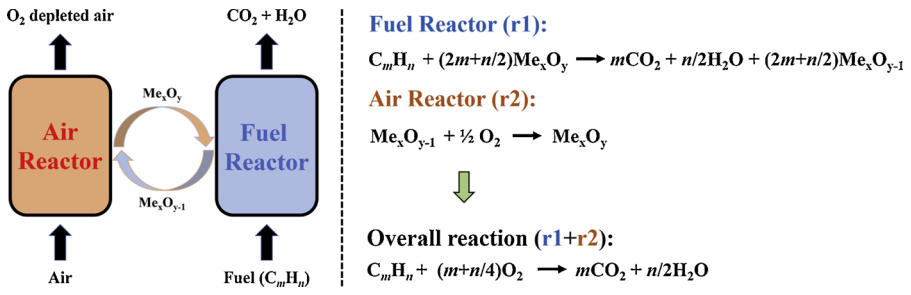

Fig. 1. Schematic and key reactions of the CLC process.

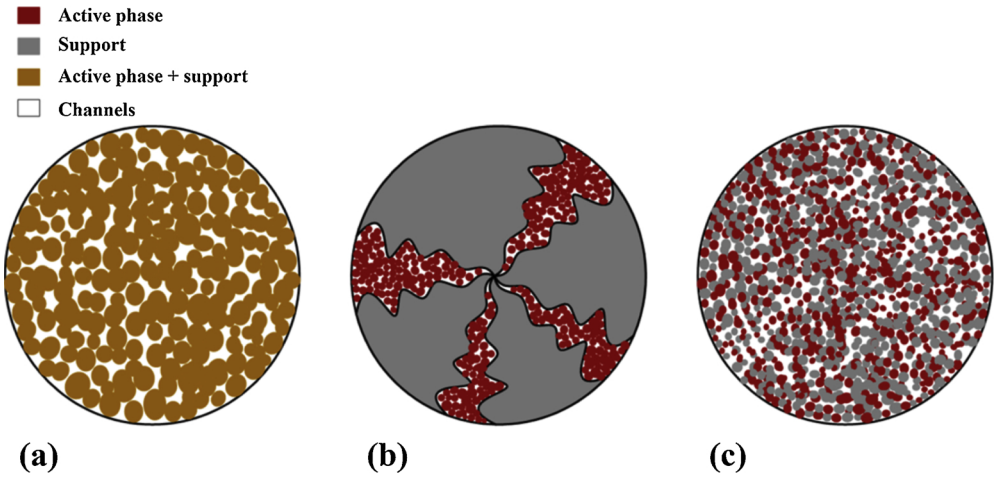

Fig. 2. Three different structures of the oxygen carrier precursor prepared by different synthesis methods (Mei et al., 2014).

also be reviewed. For the review on chemical looping reactors, experience on the design, construction, operation, and simulation of the inter-connected fluidized bed reactor will be discussed.

2. Development of oxygen carriers

2.1. Property requirements of oxygen carrier

In chemical looping processes, the oxygen carrier circulates within the inter-connected reaction system formed by the air reactor (AR) and fuel reactor (FR), continuously providing active oxygen needed for fuel conversion. Meanwhile, the oxygen carrier acts as a heat carrier, transferring generally the heat generated in AR to FR and balancing the heat difference within the whole reactor system. Therefore, the development of oxygen carriers with robust physicochemical properties is critical for the successful deployment of chemical looping processes. Generally, the suitable oxygen carrier material should meet the following stringent criteria (Adanez et al., 2012): 1) high oxygen transport capacity; 2) sufficient and regenerable redox reactivity; 3) high mechanical strength, low attrition rate, and thermal stability; 4) low cost and environmentally benign; 5) resistance to coke and other contaminants (*e.g.*, sulfur, ash, *etc.*). By now, over 1200 kinds of oxygen carriers, including Fe- (Abad et al., 2007b; Bao et al., 2013c; Johansson et al., 2004; Li et al., 2011; Shen et al., 2009b; Zhu et al., 2014), Cu- (Adánez et al., 2006; Chuang et al., 2008; Gayán et al., 2012; Luis et al., 2007; Xu et al., 2013; Zhou et al., 2015), Mn- (Abad et al., 2006; Shulman et al., 2009, 2011; Zafar et al., 2007), Ni- (Gayán et al., 2008; Linderholm et al., 2008; Mattisson et al., 2006; Shen et al., 2010a, 2009a), Co-based metal oxides (Li et al., 2008; Song et al., 2014; Zhang et al., 2009), $CaSO_4$ (Shen et al., 2008; Song et al., 2008a, b; Tian et al., 2010; Zheng et al., 2010), perovskite type materials (Galinsky et al., 2015, 2016; He et al., 2013; Leion et al., 2009b; Sarshar et al., 2011; Zhu et al., 2018a), and natural ores (Ma et al., 2019b; Matzen et al., 2017; Ströhle et al., 2015; Sundqvist et al., 2015; Wen et al., 2012; Xu et al., 2016), have been investigated by different research groups worldwide. In this article, we mainly focus on oxygen carriers originated from Fe- and Cu-based materials, including both synthetic ones and natural ores, as well as monometallic oxide and bimetallic oxides. Moreover, results of other oxygen carriers based on Ni-, Mn-, and $CaSO_4$ were also briefly reviewed and commented.

2.2. Preparation methods

Pure metal oxides usually have poor thermal stability, which are not capable of withstanding the severe cyclic redox reaction condition in chemical looping processes if used as oxygen carriers alone. To address this issue, ceramic materials (generally inert phases) were usually used to support the metal oxides (active phases). The introduction of support material can on one hand enlarge the gas-solid reaction surface area by dispersing the active phase on the support skeleton. On the other hand, the mechanical strength and attrition resistance of the attained metal oxide/support oxygen carrier system can be enhanced by the support. Eventually, both the reactivity and thermal stability of the resulted oxygen carrier are expected to improve to a certain degree. The most commonly used supports in oxygen carrier preparation include Al_2O_3, SiO_2, TiO_2, MgO, $CuAl_2O_4$, $MgAl_2O_4$, YSZ, ZrO_2, bentonite, and cement et al. As can be anticipated, the dispersing characteristic of the active phase on the support skeleton, as well as the potential chemical reaction between the active phase and support would affect the performance of the oxygen carrier. Therefore, the oxygen carrier synthesis method is of vital importance.

In general, the synthesis procedure of oxygen carrier consists of three steps: 1) preparation of the precursor, 2) drying and sintering of the obtained precursor, 3) grinding and sieving to attain fresh oxygen carrier particles. For different synthesis methods, they mainly differ in the precursors preparation step (the first step), while the last two steps are generally the same. To date, different synthesis methods have been investigated, *e.g.*, mechanical mixing (MM), sol-gel (SG), sol-gel combustion synthesis (SGCS), solid state reaction (SSR), wet impregnation (IM), co-precipitation (CP), freeze granulation (FG), spray drying (SD), hydrothermal synthesis (HS), and self-assembly template combustion synthesis (SATCS) method, *etc*. Detailed procedures of aforementioned synthesis methods have been introduced/summarized in previous publications. (Guo et al., 2014; Xu et al., 2015; Zhao et al., 2014a) For all these methods, particles with three different types of structure can be attained in the precursor preparation step, as shown in Fig. 2. To be more specific, depending on the preparation method, the structure of the precursor can possess (Mei et al., 2014): (a) a uniform structure with active and inert phases homogenously mixed at molecular level; (b) a non-uniform distribution of active and inert phases; (c) a uniform structure with active phase and inert phase distributed separately.

2.3. Applications of different oxygen carriers

Due to the varied chemical compositions and/or physical structure of different oxygen carriers, their redox reactivity, thermal stability, as well as mechanical strength can differ a lot in reaction. Additionally, when turning to large-scale application, oxygen carrier cost is another important aspect that should be carefully considered. In this sense, it is necessary to adopt different oxygen carriers accordingly in different chemical looping processes. For instance, Cu-based oxygen carriers, which show high reactivity and oxygen uncoupling characteristic, are

suitable for CLOU of solid fuels. Fe-based oxygen carriers, on the other hand, are much cheaper but exhibit relatively lower reactivity, can be applied to CLC of gaseous fuels or *i*G-CLC of coal (especially for the low-rank coal that is easy to be gasified, lignite for example). In the following part, results of oxygen carriers tested or modeled in different chemical looping processes at HUST will be comprehensively reviewed.

2.3.1. Synthetic Fe-based oxygen carriers

Due to the low cost, environmentally benign and moderate reactivity, Fe-based oxygen carriers were considered to be promising for commercial CLC application. Generally, the reduction of Fe_2O_3 with fuel gas undergoes three different reduction stages ($Fe_2O_3 \rightarrow Fe_3O_4$, $Fe_3O_4 \rightarrow FeO$, and $FeO \rightarrow Fe$). But in CLC process, only the reduction from Fe_2O_3 to Fe_3O_4 can be effectively utilized because of thermodynamic limitation. More specifically, further reduction of Fe_3O_4 to FeO or Fe will result in the increase of equilibrium partial pressure of CO and H_2 in flue gas, leading to decreased combustion efficiency and CO_2 capture efficiency.

The sol-gel combustion synthesis (SGCS) method, which combined the sol-gel technique with solution combustion synthesis, was proposed to prepare the Fe_2O_3/Al_2O_3 oxygen carrier. (Wang et al., 2011b, d; Wang et al., 2012a) Several characterization techniques, including Fourier transform infrared spectroscopy (FTIR), thermogravimetric analysis (TGA), X-ray diffraction (XRD), and N_2 isothermal adsorption/desorption methods, were adopted to characterize the prepared Fe_2O_3/Al_2O_3 oxygen carrier. (Wang et al., 2011b) The results indicated that the Fe_2O_3/Al_2O_3 oxygen carrier prepared by the SGCS method was superior in physicochemical properties. For further investigation, the SGCS-derived Fe_2O_3/Al_2O_3 oxygen carrier was tested with three Chinese coals (PDS bituminous coal, LPS lean coal, and YQ anthracite) in TGA. (Wang et al., 2011d) In comparison to the baseline results (without oxygen carrier), the reaction between Fe_2O_3/Al_2O_3 and coal underwent three stages at temperatures higher than 200 °C, ascribed to the partial pyrolysis of coal at low temperature, primary reaction and secondary reaction stages of Fe_2O_3 with coal pyrolysis products.

The physicochemical characteristics (including mechanical strength, microstructure, crystalline phase, and reactivity towards H_2) of Fe_2O_3/Al_2O_3, as prepared by different methods, were investigated and compared. (Zhao et al., 2014a) As shown in Fig. 3, XRD results indicated very similar crystalline phase of the Fe_2O_3/Al_2O_3 oxygen carriers prepared by different synthesis methods, despite the slight difference in phase intensity. Nevertheless, different preparation methods did significantly affect the activity of the resulted oxygen carriers. Among them, Fe_2O_3/Al_2O_3 prepared by the freeze granulation

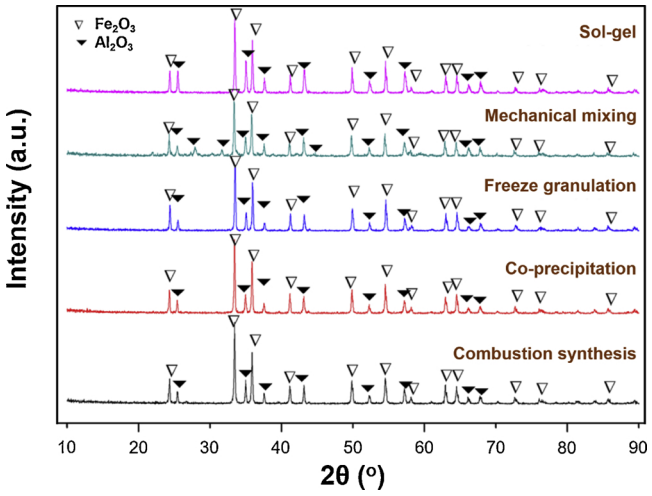

Fig. 3. XRD patterns of Fe_2O_3/Al_2O_3 oxygen carriers prepared by different methods (Zhao et al., 2014a).

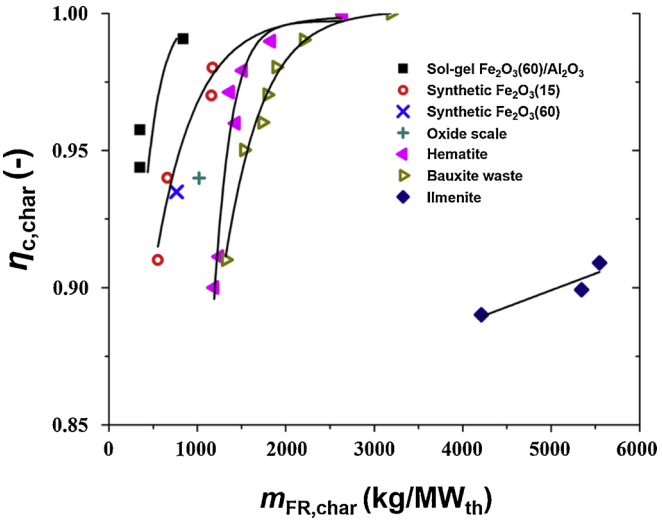

Fig. 4. Comparison of the bed inventory required for different oxygen carriers at varied char conversion. Data from published works (Abad et al., 2012b; Jerndal et al., 2011; Leion et al., 2007; Mei et al., 2014) and the reaction temperature is 900 °C.

method showed the highest H_2 conversion rate and followed by the sol-gel method. The homogeneous morphological structure attained by the freeze granulation method was believed to be the main reason of the superior activity.

The sol-gel derived Fe_2O_3/Al_2O_3 oxygen carrier was evaluated in *i*G-CLC process, using lignite (from Xiaolongtan, China) as fuel and steam as gasification agent. (Mei et al., 2014) Steam content was found to exert little impact on the conversion of volatiles, while significantly promoted the gasification of lignite char. The overall conversion rate of lignite in FR was limited by the char gasification process, which could be enhanced by operating at higher temperatures. Moreover, a higher solid inventory in FR was generally beneficial to attaining higher char conversion efficiency. As shown in Fig. 4, when compared with literature results, the sol-gel derived Fe_2O_3/Al_2O_3 oxygen carrier enabled an extremely low solid inventory of 600 kg/MW_{th} in FR to achieve 99 % char combustion at 900 °C. High sintering resistance and physical stability of the oxygen carrier were also observed, which all together indicated that the sol-gel derived Fe_2O_3/Al_2O_3 is highly promising in *i*G-CLC process.

Fe_2O_3/Al_2O_3 oxygen carrier prepared by the co-precipitation method was further applied to chemical looping dechlorination of plastic waste, aiming to achieve *in-situ* inhibition of dioxins. (Wang and Zhao, 2015) High dechlorination efficiency can be achieved when Fe_2O_3/Al_2O_3 was decorated by CaO. The effects of different CaO decoration method (mechanical mixing, wet impregnation, or co-precipitation), CaO loading ratio (5 – 15 wt.%), and reaction temperature (850 – 925 °C) on the dechlorination performance of the oxygen carrier were investigated in a batch fluidized reactor. It turned out that 5 wt.% of CaO promotion onto the Fe_2O_3/Al_2O_3 *via* wet impregnation could achieve the highest dechlorination efficiency. A higher reaction temperature was generally beneficial for dechlorination but would lead to more severe carbon deposition at the surface of the oxygen carrier and thus lower combustion efficiency. Environmental scanning electron microscope coupled with energy dispersive X-ray (ESEM-EDX) analysis indicated Cl accumulation at the surface of the cycled particles, resulting in gradually decreased dechlorination efficiency. Nevertheless, diluted hydrochloric acid solution was found to be effective to refresh the cycled oxygen carrier by eliminating these hydrosoluble Ca and Cl from the surface, and this was confirmed by ESEM-EDX analysis. As a follow up, the feasibility of using chemical looping concept for *in-situ* inhibition of polychlorinated dibenzo-p-dioxins and dibenzofurans (PCDD/Fs) was further evaluated by investigating the distribution of 17

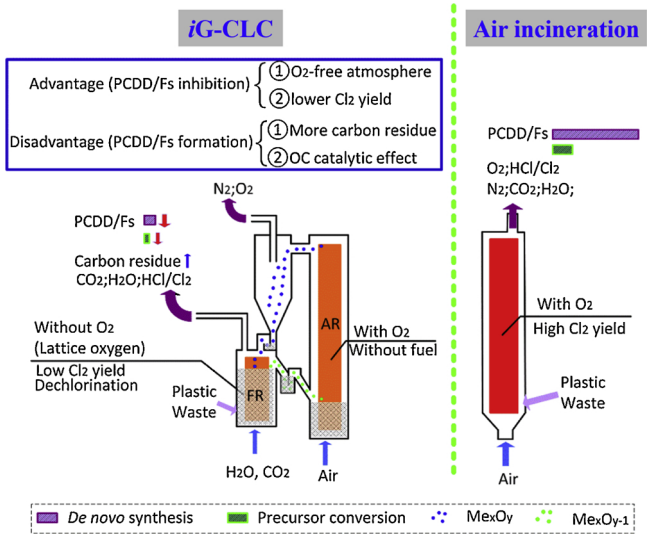

Fig. 5. PCDD/Fs formation and inhibition mechanisms in *i*G-CLC of plastic waste. (Zhao and Wang, 2018).

toxic PCDD/Fs congeners as well as their formation and inhibition mechanism in *i*G-CLC of plastic waste. (Zhao and Wang, 2018) In comparison to conventional air incineration process, *i*G-CLC of plastic waste with CaO-decorated Fe_2O_3/Al_2O_3 as oxygen carrier was found to be able to reduce the total amount and toxic equivalency of PCDD/Fs by 94 % and 89, respectively. To be more specific, the inhibition mechanisms of PCDD/Fs in *i*G-CLC process were revealed and summarized, as shown in Fig. 5: 1) the O_2-free environment in CLC process significantly inhibits the *de novo* synthesis of PCDD/Fs; 2) lower Cl_2 formation (due to the limitation of Deacon reaction in O_2-free condition) and the suppressed precursor conversion as well as *de novo* synthesis of PCDD/Fs due to the dechlorination capability of the CaO-decorated Fe_2O_3/Al_2O_3 oxygen carrier. Chlorine substitution modelling was also conducted, which reproduced the experimental results well and further demonstrated that the chlorine substitution probabilities for the formation of 7 toxic PCDDs congeners and 10 toxic PCDFs congeners were indeed significantly decreased in *i*G-CLC process.

Most of the synthetic oxygen carriers studied in literatures were prepared in lab-scale. However, considering the large amount of oxygen carrier requirement in commercial chemical looping reactors, oxygen carrier production in large-scale is more desirable from both efficiency and economy standpoints. Several potential large-scale production methods, including freeze granulation, spray drying, impregnation, and mechanical mixing have been investigated (Guo et al., 2014) To evaluate the pros and cons of different preparation methods, the synthesis of Fe_2O_3/Al_2O_3 oxygen carrier was adopted for comparison, mainly focused on the productivity, production cycle, physicochemical characteristic, and reactivity towards lignite. As shown in Table 1, the Fe_2O_3/Al_2O_3 oxygen carrier prepared by the freeze granulation method exhibits high productivity, high crushing strength, and low attrition rate. Further tests of this oxygen carrier in a batch fluidized bed reactor with lignite as fuel showed the highest carbon conversion rate, which suggested that the freeze granulation method would be appropriate for large-scale oxygen carrier production. Nevertheless, we should note here that spray drying is the most commonly used method for large-scale oxygen carrier production, which might indicate that the spray drying procedure adopted in this work needs further optimization.

Different synthetic Fe-based oxygen carriers reviewed above are summarized in Table 2. As it can be seen, most of these oxygen carriers were prepared with Al_2O_3 as inert support, and were adopted either in CLC or *i*G-CLC process. TGA and batch fluidized bed reactor were generally used for oxygen carrier activity evaluation, using gaseous and/or solid fuels as reactants. Among different preparation methods, Fe_2O_3/Al_2O_3 synthesized *via* the sol-gel method was proved to exhibit the highest activity, and it has been demonstrated to be a promising oxygen carrier for application in *i*G-CLC of low rank coal.

2.3.2. Synthetic Cu-based oxygen carriers

Due to the capability of releasing gaseous O_2 at high temperature and appropriate O_2 partial pressure, Cu-based oxygen carriers were suitable for the conversion of solid fuels, like coal, petroleum coke, and biomass. Nevertheless, the easy-to-sintering issue of CuO at high temperature should be resolved before application in chemical looping processes. $CuAl_2O_4$, which shows merits of high melting point, thermal stability, and corrosion resistance, was verified to be an appropriate support for CuO. (Mei et al., 2013b) On the other side, $CuAl_2O_4$ was also demonstrated as a promising oxygen carrier for CLC of gaseous fuels. (Arjmand et al., 2012) The oxygen release capability as well as the reactivity towards three Chinese coals with different ranks (lignite, bituminous, and anthracite) of a sol-gel-derived $CuO/CuAl_2O_4$ oxygen carrier was studied in a batch fluidized bed reactor. The effects of coal rank and reaction temperature on the CLOU performance were analyzed. Generally, higher carbon conversion rate can be achieved for the lower rank coal, and the conversion rate of higher rank coal were more sensitive to the increase of reaction temperature. Almost complete conversion can be achieved for all the three coals, and no carbon deposition occurred to the used oxygen carrier. Nevertheless, slight sintering issue occurred when lignite was used as fuel.

Well-organized TGA tests were then conducted to illustrate the relevance of gas-solid reaction and oxygen uncoupling of the $CuO/CuAl_2O_4$ oxygen carrier with gaseous fuels. (Mei et al., 2015a) Cyclic oxygen release and uptake tests indicated that CuO was able to fully decompose into Cu_2O in N_2 and then regenerate back to CuO in air, but the decomposition process of $CuAl_2O_4$ was very slow and the subsequent regeneration step was difficult to complete. When using the $CuO/CuAl_2O_4$ oxygen carrier for gaseous fuels, the reaction mode, either CLOU or CLC dominated, can be distinguished by the concentration of fuel gas. As shown in Fig. 6, for the conversion of H_2, a critical value of 1 vol.% was observed: when the H_2 concentration was lower than 1 vol.%, oxygen decoupling of the oxygen carrier was more significant than the gas-solid reaction of CuO with H_2, thus in the CLOU reaction mode; when it was higher than 1 vol.%, the reaction between CuO and H_2 was the dominant reaction and therefore processed in the CLC mode.

The $CuO/CuAl_2O_4$ oxygen carrier was further tested in chemical looping gasification (CLG) of biomass for syngas production, which showed advantages of high carbon conversion, low C_2H_m yield, and tar removal. (Zhao et al., 2015) However, due to the high reactivity of $CuO/CuAl_2O_4$ oxygen carrier, large proportion of CO_2 was produced in

Table 1
Productivity, production cycle, and physical properties of the Fe_2O_3/Al_2O_3 oxygen carriers prepared by different methods. (Guo et al., 2014).

Preparation method	Productivity χ (%)	Production cycle T (h)	Surface area ($m^2\ g^{-1}$)	Crushing strength (N)	Attrition index K_a (%)
Freeze granulation	38.62	37	1.99	5.1 ± 0.3	5.1
Spray drying	15.52	20	1.93	2.7 ± 0.1	8.0
Impregnation	40.63	29	1.59	1.9 ± 0.2	17.4
Mechanical mixing	32.12	39	2.03	1.5 ± 0.2	12.7

Table 2
Summary of synthetic Fe-based oxygen carriers for chemical looping.

Fe_2O_3 content (wt.%)	Support material	Preparation method	Application	Facility	Reacting agent	Ref.
61.1	Al_2O_3	SGCS	CLC	TG-FTIR	H_2, O_2	(Wang et al., 2011b)
80	Al_2O_3	SGCS	CLC	TG-FTIR	Coals, O_2	(Wang et al., 2011d)
80	Al_2O_3	SGCS	CLC	TG-FTIR	Anthracite, O_2	(Wang et al., 2012a)
60	Al_2O_3	SG, CP, SSR, HS, MM, CS, FG	CLC	TGA	H_2, O_2	(Zhao et al., 2014a)
60	Al_2O_3	SG	*i*G-CLC	b-FB	Lignite, O_2	(Mei et al., 2014)
60	Al_2O_3, ($CaO/Na_2O/K_2O$) [a]	CP	CLC, *i*G-CLC	TGA, b-FB	HCl-containing synthesis gas, medical plastic waste, O_2	(Wang and Zhao, 2015)
60	Al_2O_3, (CaO) [a]	CP	*i*G-CLC	b-FB	Medical plastic waste, O_2	(Zhao and Wang, 2018)
60	Al_2O_3	FG, SD, MM, IM	CLC	b-FB	Lignite, O_2	(Guo et al., 2014)

Notes: [a] dopant; b-FB, batch fluidized bed reactor.

the reforming process, thus degraded the value of the reforming gas products to a certain degree. Nevertheless, the generation of CO_2, which was attributed to the full oxidation reaction between CuO and reducing gases, was exothermic; while the biomass reforming process was endothermic. In this regard, auto-thermal operation can be potentially achieved once the reactions in the FR of CLG were properly tuned. Further work to optimize the experimental condition as well as the oxygen carrier composition is essential to improve the syngas selectivity.

The effect of different supports (TiO_2, ZrO_2, $CuAl_2O_4$, and $MgAl_2O_4$) on the performance of Cu-based oxygen carrier was investigated *via* DFT calculation, thermo-mechanical analysis (TMA), and isothermal oxygen decoupling test in TGA. (Zhao et al., 2017) DFT calculation indicated that CuO/$MgAl_2O_4$ was the most sintering-resistant, followed by CuO/ZrO_2, CuO/$CuAl_2O_4$, and CuO/TiO_2. The calculation results agreed well with the experimental values (glass transition temperature, which could be an indicator of the sintering resistance of solid material) measured by TMA. The energy barriers for the oxygen release and adsorption stages of CuO/$MgAl_2O_4$, CuO/$CuAl_2O_4$, CuO/ZrO_2, and CuO/TiO_2 are shown in Fig. 7. As it can be seen, CuO/TiO_2 shows the lowest energy barriers in both oxygen formation and desorption steps among the four Cu-based oxygen carriers. To sum up, TiO_2 was the most promising inert support for CuO from reactivity standpoint, but not the case in sintering resistance.

To improve the anti-sintering property of the CuO/TiO_2 oxygen carrier, Al_2O_3 was further added to TiO_2 to form a composite inert support, *i.e.*, TiO_2-Al_2O_3. Using the SATCS method, core-shell structured CuO@TiO_2-Al_2O_3 oxygen carrier (with 77.5 wt.% CuO, 17.5 wt.% Al_2O_3, and 5 wt.% TiO_2) was prepared. (Xu et al., 2015) During the synthesis, the support material was selected based on DFT calculation and the particle size of the inert material was optimized according to the Zener pinning theory. The aggregation between Al_2O_3 and TiO_2 to

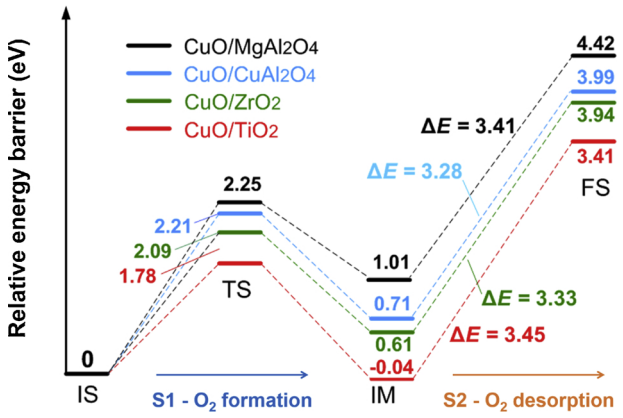

Fig. 7. Potential energy profiles of the oxygen release process for CuO/$MgAl_2O_4$, CuO/$CuAl_2O_4$, CuO/ZrO_2, and CuO/TiO_2 oxygen carriers, corresponding energy barriers for O_2 formation and O_2 desorption steps. (Zhao et al., 2017).

form core (Al_2O_3)-shell (TiO_2) template was driven by the van der Waals attractive and electrostatic attractive forces spontaneously. Population Balance Monte Carlo (PBMC) simulation was also employed to directly track the complicated multicomponent aggregation, including hetero-aggregation (nano-TiO_2 coating on the surface of micro-Al_2O_3) and homo-aggregation (Al_2O_3-Al_2O_3, TiO_2-TiO_2) in aqueous suspensions. (Zhao et al., 2019) PBMC simulation can help to understand the competitive mechanisms of particle-particle interactions and then rationalize the oxygen carrier preparation parameters (*e.g.*, pH value and ionic strength), so as to attain the Al_2O_3@TiO_2 core-shell microarchitecture with a good coverage efficiency and a moderate shell thickness. Fig. 8 gives a schematic view of the synthesis procedure of

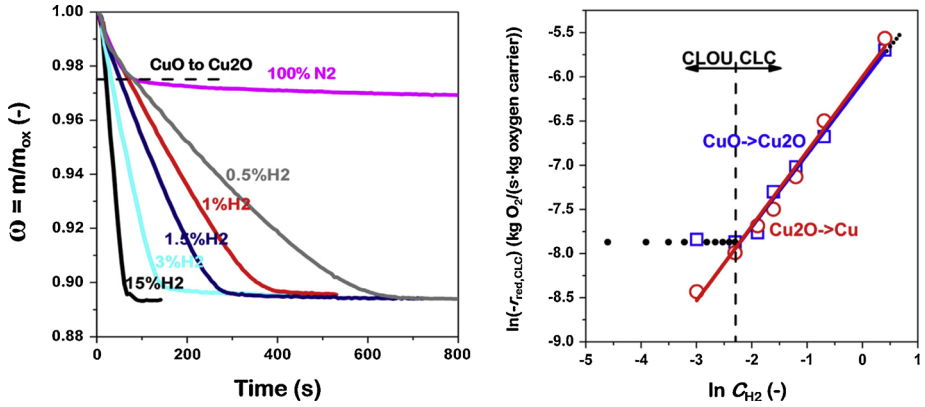

Fig. 6. Effect of H_2 concentration on the reaction mode of CuO/$CuAl_2O_4$ oxygen carrier in chemical looping. Reaction temperature: 950 °C. (Mei et al., 2015a).

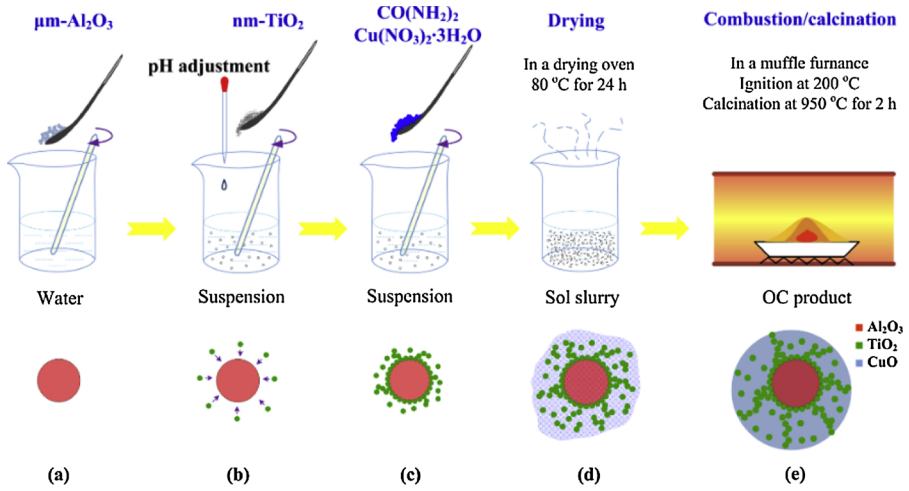

Fig. 8. A schematic view of the synthesis procedure of the CuO@TiO_2-Al_2O_3 oxygen carrier *via* the SATCS method. (Xu et al., 2015).

the SATCS method. Generally, the synthesis process can be divided into four sub-steps: I) Calculated amount of μm-Al_2O_3 and nm-TiO_2 were evenly dispersed in deionized water at 80 °C and the pH value of the suspension was adjusted to 6; II) Urea ($CO(NH_2)_2$) and copper nitrate trihydrate ($Cu(NO_3)_2{\cdot}3H_2O$) were added into the slurry sequentially to form a gel-like precursor; III) The wet gel was dried in an oven overnight and then ignited in a muffle furnace; IV) Finally, the as-burned precursor was calcined at 950 °C for 2 h to obtain the oxygen carrier product. More details of the preparation process can be found elsewhere. (Tian et al., 2017b, 2018b; Xu et al., 2015) Note that, the nm-TiO_2 particles used was prepared by flame synthesis technique in lab (Xu et al., 2015, 2017), and more details of the synthesis process will be introduced in **Part 2.4**. Additionally, the SATCS method was praised for its zero NO_x emission during the combustion synthesis process, attributing to the reaction of R9. In this sense, green synthesis of the CuO@TiO_2-Al_2O_3 oxygen carrier from nitrate precursors was realized.

$$3Cu(NO_3)_2+5CO(NH_2)_2 \rightarrow 3CuO+5CO+10H_2O+8N_2 \quad (R9)$$

Performance of the CuO@TiO_2-Al_2O_3 oxygen carrier was evaluated for different applications under the context of chemical looping. (Tian et al., 2017b, 2018b; Xu et al., 2015) The oxygen carrying capacity, cyclic oxygen release and uptake characteristics, and reactivity towards CH_4 were first investigated. (Xu et al., 2015) Oxygen decoupling tests at 900 °C showed an oxygen release rate of up to 0.37 g O_2/(g oxygen carrier) per min, which was 11 and 18 times higher than those of CuO/Al_2O_3 (80 wt.% CuO, at 950 °C) (Imtiaz et al., 2014) and CuO/TiO_2 (50 wt.% CuO at 900 °C) (Clayton and Whitty, 2014), respectively. According to SEM and XRD analyses of both fresh and used samples, the TiO_2-Al_2O_3 composite inert support was found to be superior in two aspects: on the one hand, the addition of Al_2O_3 increased the sintering resistance of the resulted oxygen carrier; on the other hand, the presence of nm-TiO_2 on the surface of Al_2O_3 suppressed the direct contact between CuO and Al_2O_3, thus limited the formation of $CuAl_2O_4$ spinel. These also explained the high reactivity and physical stability of the CuO@TiO_2-Al_2O_3 oxygen carrier.

CLOU characteristic of the CuO@TiO_2-Al_2O_3 oxygen carrier with coal was then investigated in a batch fluidized bed reactor. (Tian et al., 2017b) During the 20 redox cycles with GP anthracite as fuel, combustion efficiency of up to 97.2 % was achieved. XRD analysis of the cycled samples indicated no $CuAl_2O_4$ spinel phase formation, and porous surface morphology of the particle was well preserved according to SEM results.

Considering the high oxygen capacity as well as the fast oxygen release rate, further application of the CuO@TiO_2-Al_2O_3 oxygen carrier to CLAS was demonstrated in a paralleled fluidized bed reactor. (Tian et al., 2018b) H_2O/CO_2 was used as the carrier gas during the O_2 decoupling step, and air was introduced to recuperate the reduced oxygen carrier. During 10 h of continuous running, stable O_2/CO_2 stream with O_2 concentration in the range of 19.7–27.6 vol.% (steam free basis) was attained and no obvious activity degradation occurred (as shown in Fig. 9). For the case of 100 g of oxygen carrier inventory in each reactor, an average O_2 production rate of 3.34×10^{-7} mol/s per gram oxygen carrier was achieved, which was higher than literature results under similar operation condition. (Wang et al., 2016d) Note that, the O_2 concentration in the outlet gas flow was adjustable by changing the H_2O/CO_2 ratio in the inlet gas, and pure O_2 could be attained if only steam was used as the carrier gas.

Table 3 summarizes the application of different synthetic Cu-based oxygen carriers in chemical looping processes. Among them, the CuO@TiO_2-Al_2O_3 oxygen carrier prepared by the SATCS method was highly reactive towards both gaseous fuel and coal. Moreover, the superior oxygen decoupling and regeneration properties made it very promising for O_2 production.

2.3.3. *Synthetic bimetallic oxygen carriers*

Usually, single-phase metal oxide is difficult to meet all the criteria required by an oxygen carrier. For example, Fe-based oxygen carriers are generally cheap and non-toxic, but they show relatively low activity towards solid fuels. Cu-based oxygen carriers, on the other hand, exhibit oxygen uncoupling ability and high activity, yet are prone to

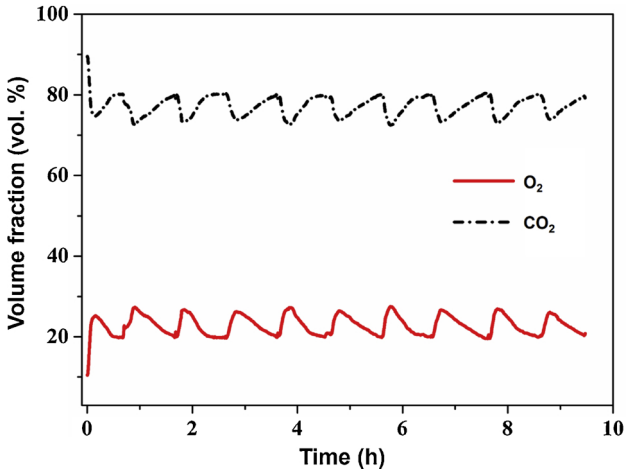

Fig. 9. Continuous O_2/CO_2 stream (steam free basis) production with CuO@TiO_2-Al_2O_3 as oxygen carrier at 950 °C in the paralleled fluidized bed reactor. (Tian et al., 2018b).

Table 3
Summary of synthetic Cu-based oxygen carriers for chemical looping.

CuO content (wt.%)	Support material	Preparation method	Application	Facility	Reacting agent	Ref.
60	$CuAl_2O_4$	SG	CLOU	b-FB	Coals, O_2	(Mei et al., 2013b)
21.9	$CuAl_2O_4$	SG	CLC, CLOU	TGA	H_2, CH_4, O_2	(Mei et al., 2015a)
60	$CuAl_2O_4$	SG	CLR	b-FB	Pine sawdust, O_2	(Zhao et al., 2015)
77.5	TiO_2-Al_2O_3	SATCS	CLC, CLOU	TGA, b-FB	H_2, CH_4, O_2	(Xu et al., 2015)
77.5	TiO_2-Al_2O_3	SATCS	CLC, CLOU	TGA, b-FB	H_2, Coal, O_2	(Tian et al., 2017b)
77.5	TiO_2-Al_2O_3	SATCS	CLAS	TGA, p-FB	H_2O/CO_2, O_2	(Tian et al., 2018b)

Notes: b-FB, batch fluidized bed reactor; p-FB, paralleled fluidized bed reactor.

sintering and agglomeration at elevated temperature. To resolve this contradiction, researchers came up with the idea of using mixed oxides as oxygen carrier. The main objective of using bimetallic oxide rather than single-phase metal oxide is to integrate the merits of different metal oxides, so as to enhance the overall reaction performance of the resulted oxygen carrier. Investigations on bimetallic oxygen carriers were conducted either by mixing different metal oxides mechanically or by forming bimetallic compound in a single particle.

$CuFe_2O_4$ was proposed as a novel oxygen carrier for CLC of coal (Wang et al., 2011c) By integrating the Cu and Fe cations into one oxide matrix, $CuFe_2O_4$ was expected to show superior physiochemical characteristics over CuO or Fe_2O_3. TG-FTIR was used to investigate the reaction of $CuFe_2O_4$ with two Chinese coals (LPS sub-bituminous and YQ anthracite), and satisfying performance of the bimetallic oxygen carrier was indeed attained. The results demonstrated two reaction stages for LPS coal, at 300 − 600 °C and 600 − 850 °C, respectively; while only one distinct reaction stage was observed for the reaction with YQ coal, at above 600 °C. The difference could be mainly attributed to the different volatile contents of the two coals. At temperatures higher than 800 °C, $CuFe_2O_4$ would decompose into $CuFeO_2$ and then Cu_2O, releasing O_2 at the same time, which was beneficial to the conversion of char and combustible gases. Thermodynamic simulation results showed that iron silicates would form by side reactions between coal ash and the reduced $CuFe_2O_4$, leading to insufficient regeneration capability of the reduced $CuFe_2O_4$. Therefore, effective ash separation is critical in CLC of coal. Subsequently, performance of the $CuFe_2O_4$ oxygen carrier with a high-sulfur petroleum coke (JS) was evaluated. (Wang et al., 2013a) It was found that the reactivity of $CuFe_2O_4$ with JS coke was comparable to that of CuO. Physicochemical characterizations, including SEM-EDX and XRD, indicated that $CuFe_2O_4$ was mainly reduced to Cu and Fe_3O_4 in the reaction, as also being verified by thermodynamic simulation results. For the organic sulfur in JS coke, over 90 % of which reacted with $CuFe_2O_4$ and formed solid Cu_2S. Side reaction products, like Cu_2S, Fe_2SiO_4 and $FeSiO_3$, should be responsible for the incomplete conversion of JS coke.

Furthermore, mixed CuO/Fe_2O_3 oxygen carrier was proposed for CLG of biomass. (Niu et al., 2018) By using the sol-gel combustion synthesis method, bimetallic Cu-Fe oxides with different CuO/Fe_2O_3 molar ratios were prepared. TGA tests with sawdust as feedstock were first conducted to evaluate the reforming performance of the bimetallic Cu-Fe oxygen carriers. As indicated, a higher CuO loading ratio was generally beneficial to achieving superior activity towards sawdust. The CuO/Fe_2O_3 molar ratio was optimized by further tests in a batch fluidized bed reactor, and the optimum value was attained as 1:1, based on the comprehensive consideration of gas product distribution, syngas yield, carbon conversion, and tar yield. Moreover, the effects of reaction temperature, steam to biomass ratio (S/B), and oxygen carrier to biomass ratio (O/B) were systematically investigated, using the Cu5Fe5 (molar ratio of CuO/Fe_2O_3 equaled to 1) as oxygen carrier. The most promising result was attained under the condition of 800 °C, S/B = 0.75, and O/B = 0.2.

Chemical looping was proved to be a promising way for tar removal in biomass treatment. (Lind et al., 2011) In the follow up work, the tar generated in the sawdust-derived CLG process was measured and quantified by Gas Chromatography-Mass Spectrometer (GC–MS). (Tian et al., 2018a) The tests were conducted in a batch fluidized bed reactor, using Cu5Fe5 as oxygen carrier and operated at the optimal experimental conditions attained in previous work. (Niu et al., 2018) It was found that the molar weight of compounds in tar were mostly around 200. The Cu content in the Cu-Fe bimetallic oxygen carrier was beneficial to decreasing the yield of small molecular compounds, while the Fe content could promote the decomposition of large molecular compounds.

Besides $CuFe_2O_4$, several other bimetallic oxygen carriers, including $NiFe_2O_4$, $MnFe_2O_4$, and $CoFe_2O_4$, were also investigated. (Wang et al., 2014a, b; Wang et al., 2012b) All these samples were synthesized *via* the sol-gel combustion synthesis method and tested either with a high-sulfur coal (from Liuzhi, China, LZ) or with H_2 in TGA. Several characterization methods, including FTIR, SEM-EDX, and XRD were adopted to investigate the sulfur fate as well as the effect of sulfur compounds on oxygen carrier. TG-FTIR analysis indicated two stages of the reaction between LZ coal and $NiFe_2O_4$ oxygen carrier, at 350 − 550 °C and 800 − 900 °C, respectively. Moreover, much higher oxygen transfer rate was attained by $NiFe_2O_4$ in comparison to directly mixed NiO/Fe_2O_3 oxygen carrier during the reaction with LZ coal. The evolution of SO_2 was mainly ascribed to the oxidation of H_2S by $NiFe_2O_4$ at temperatures higher than 550 °C. Thermodynamic simulation and XRD characterization results showed that the main reduction products of $NiFe_2O_4$ were Ni and Fe_3O_4. Ni_3S_2 resulted from side reaction was also observed, yet complete regeneration of the reduced $NiFe_2O_4$ oxygen carrier could still be attained.

More recently, CaO/Fe_2O_3 (calcium ferrite) was adopted as oxygen carrier in CLG of coal/char for syngas production. (Wang et al., 2019) In the batch fluidized bed tests with SL lignite as feedstock, the molar ratio of CaO to Fe_2O_3 in the calcium ferrite oxygen carrier was varied from 0:1 to 0.7:0.3 for optimization. It turned out that the highest H_2/CO ratio and syngas yield were attained as 4.6 and 1.4 Nm^3/kg coal, respectively, when the CaO/Fe_2O_3 was 0.5:0.5. $Ca_2Fe_2O_5$ was found to be a catalytic substance in the oxygen carrier, and its catalytic effect became prominent at the later stage of coal conversion when the lattice oxygen donation capability of oxygen carrier decreased.

As shown in Table 4, performance of different synthetic bimetallic oxygen carriers was summarized and compared. As it can be seen, all these bimetallic oxygen carriers were prepared by the sol-gel combustion synthesis method, and tested with solid fuels (coal, biomass or petroleum coke). The CuO/Fe_2O_3 oxygen carrier was found to be feasible in both CLC and CLG processes.

2.3.4. Natural ore oxygen carriers

For the conversion of solid fuels, reactivity degradation of the oxygen carrier by contaminants (like sulfur compounds) as well as the potential loss of solid particles from oxygen carrier/ash separation process will increase the operational cost to some extent. In this sense, for commercial application, it is necessary to use an oxygen carrier that is both economy feasible and reactivity sufficient. Due to the low cost, abundant reserves and moderate reactivity, increasing interests are

Table 4
Summary of synthetic bimetallic oxygen carriers for chemical looping.

Metal oxide 1 (wt.%)	Metal oxide 2 (wt.%)	Preparation method	Application	Facility	Reacting agent	Ref.
$CuFe_2O_4$ (100)	–	SGCS	CLC	TG-FTIR	Coals, O_2	(Wang et al., 2011c)
$CuFe_2O_4$ (100)	–	SGCS	CLC	TGA	Petroleum coke, O_2	(Wang et al., 2013a)
CuO (33.3)	Fe_2O_3 (66.6)	SGCS	CLG	TGA, b-FB	Pine sawdust, O_2	(Niu et al., 2018; Tian et al., 2018a)
CaO (0-70)	Fe_2O_3 (30-100)	IM	CLG	b-FB	Coal/char, O_2	(Wang et al., 2019)
$NiFe_2O_4$ (100)	–	SGCS	CLC	TG-FTIR	Coal, O_2	(Wang et al., 2014b)
$MnFe_2O_4$ (100)	–	SGCS	CLC	TG-FTIR	Coal, O_2	(Wang et al., 2014a)
$CoFe_2O_4$ (100)	–	SGCS	CLC	TG-FTIR	Coal, O_2	(Wang et al., 2012b)

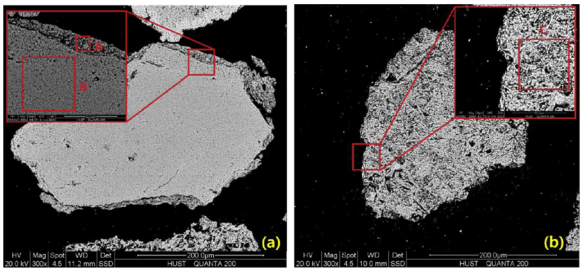

Fig. 10. SEM-EDX images of cross-cut 6CuHem particles: (a) fresh and (b) after 29 redox cycles. (Yang et al., 2014).

being shown on natural mineral materials as oxygen carriers.

2.3.4.1. Iron ore. Iron ore has been widely adopted as oxygen carrier in CLC. (Gu et al., 2012; Leion et al., 2009a; Linderholm and Schmitz, 2016; Mendiara et al., 2013; Xiao et al., 2010) Generally, the used iron ore oxygen carriers in chemical looping were mainly originated from ilmenite and hematite. Ilmenite, with the main active phase of Fe_2TiO_5, has been extensively investigated as oxygen carrier by many groups, and promising results were attained (Abad et al., 2011; Adánez et al., 2010; Bao et al., 2013a). The iron ore oxygen carrier investigated at HUST was hematite, which contained Fe_2O_3 as the active component. Due to the different origins, the properties of different kinds of hematite may vary a lot, which would eventually affect their performance in reaction. Two kinds of hematite, originated from Australia (AH) and China (CH), respectively, were comparatively studied in a batch fluidized bed reactor within the temperature range of 900 − 1000 °C. (Ma et al., 2017a) Two low-rank coals, Victorian brown coal from Australia and Inner Mongolia lignite from China, were used as solid fuels. Either CO_2/N_2 or H_2O/N_2 was used as the fluidization agent during the reduction stage. The results showed that the CH oxygen carrier (contained 65.9 wt.% of Fe_2O_3) exhibited much higher reactivity than that of AH oxygen carrier (contained 91.6 wt.% of Fe_2O_3) under the same experimental condition. In this sense, the amount of active phase in hematite was not the only determinant for oxygen carrier activity. The inert phases in hematite were found to be helpful to maintaining the porous structure of the oxygen carrier. BET analysis of both fresh and used AH and CH samples indicated larger surface area of CH than that of AH, which might explain the superior reactivity of CH over AH.

In addition, performance of the CH oxygen carrier was further evaluated in a 5 kW_{th} inter-connected fluidized bed reactor (Ma et al., 2015a, b), using CH_4 and coal as fuels. For the test fueled with CH_4 (Ma et al., 2015b), over 100 h of continuous running was achieved, with the thermal power input in the range of 1.0–1.5 kW_{th}. During the continuous operation, the CH_4 conversion achieved the highest of 81.4 % at 1000 °C. SEM characterization indicated that no sintering issue occurred to the used hematite particles. The same batch of hematite was also continuously tested with coal in the 5 kW_{th} CLC reactor. (Ma et al., 2015a) CO_2/N_2 was used as the fluidization gas as well as gasification agent during the reduction stage, running in the *i*G-CLC mode. The highest coal combustion efficiency was achieved as 96.3 %, while the CO_2 capture efficiency ranged between 72.8 and 89.4 %. No obvious ash deposition or coke was observed at the surface of the tested samples.

Even though iron ore exhibits satisfying reactivity in CLC, it still has much space for improvement. Foreign ion introduction was proved to be a good way for reactivity promotion of the raw iron ore. Cu-decorated hematite, prepared by the wet impregnation method, was used as oxygen carrier for *i*G-CLC of coal. (Yang et al., 2014) The effects of Cu loading ratio (3 − 10 wt.%), temperature (850 − 950 °C), oxygen to fuel ratio (1.0–3.0), and coal type (SH bituminous coal and GP anthracite) on the CLC performance of the Cu-decorated hematite were investigated. It turned out that the hematite with 6 wt.% of Cu decoration (6CuHem for short) showed the highest activity towards coal gasification products. Complete and fast coal conversion was achieved at temperatures higher than 900 °C. The increase of oxygen to fuel ratio was found to be beneficial for higher carbon conversion and coal combustion efficiency. As shown in Fig. 10, SEM-EDX analysis illustrated a Cu-rich shell at the surface of the fresh Cu-decorated hematite particles. However, this Cu-rich shell almost disappeared after 29 redox cycles, due to the surface abrasion and inward migration of Cu cation into the particle. The particle surface abrasion was confirmed by the decreased Cu/Fe ratio of the used sample in comparison to the fresh one (0.089 *vs.* 0.11), and the inward Cu migration was verified by the higher Cu/Fe ratio inside the used particle than that inside the fresh one (0.14 *vs.* 0.094). Nevertheless, the change of surface Cu content did not seem to affect the activity of the oxygen carrier significantly, as indicated by the stable carbon conversion rate attained in multiple redox cycles.

CaO-decorated iron ore was adopted as oxygen carrier for CLC of plastic waste, which turned out to be an ideal approach for *in situ* dechlorination in plastic waste treatment. (Wang and Zhao, 2016) For the investigation, HCl-containing synthesis gas (1 vol.% HCl, 21.9 vol.% CO, 5.9 vol.% CH_4, 12.7 vol.% H_2, 7.8 vol.% CO_2, and 50.7 vol.% N_2) was used as a model gaseous fuel. Different decoration methods (wet impregnation or ultrasonic impregnation) and CaO loading ratios were compared. The results indicated that the iron ore decorated by 5 wt.% of CaO *via* ultrasonic impregnation method could attain the highest dechlorination efficiency. Then, *i*G-CLC test of plastic waste with the CaO-decorated iron ore oxygen carrier was conducted in a batch fluidized bed reactor at different oxygen to fuel ratios. It was found that a higher oxygen to fuel ratio was generally beneficial for a higher combustion efficiency. Moreover, when the oxygen to fuel ratio was 2.5, the adverse effect of CaO decoration on the combustion efficiency of plastic waste could be effectively mitigated.

Up to now, *i*G-CLC of plastic waste has only been demonstrated in the batch fluidized bed reactor. To better simulate the practical operation, while avoiding the complexity of running an inter-connected fluidized bed reactor, a semi-continuously operated fluidized bed reactor was designed and operated. (Ma et al., 2019c) As noted, the proposed semi-continuously operated fluidized bed reactor only simulated the fuel reactor of the real *i*G-CLC system, as shown in Fig. 11. Iron ore promoted by 5 wt.% of CaO *via* the ultrasonic impregnation method was chosen as the oxygen carrier. Before formal tests, the relevance of bed inventory to gas flow rate, as well as the relationship

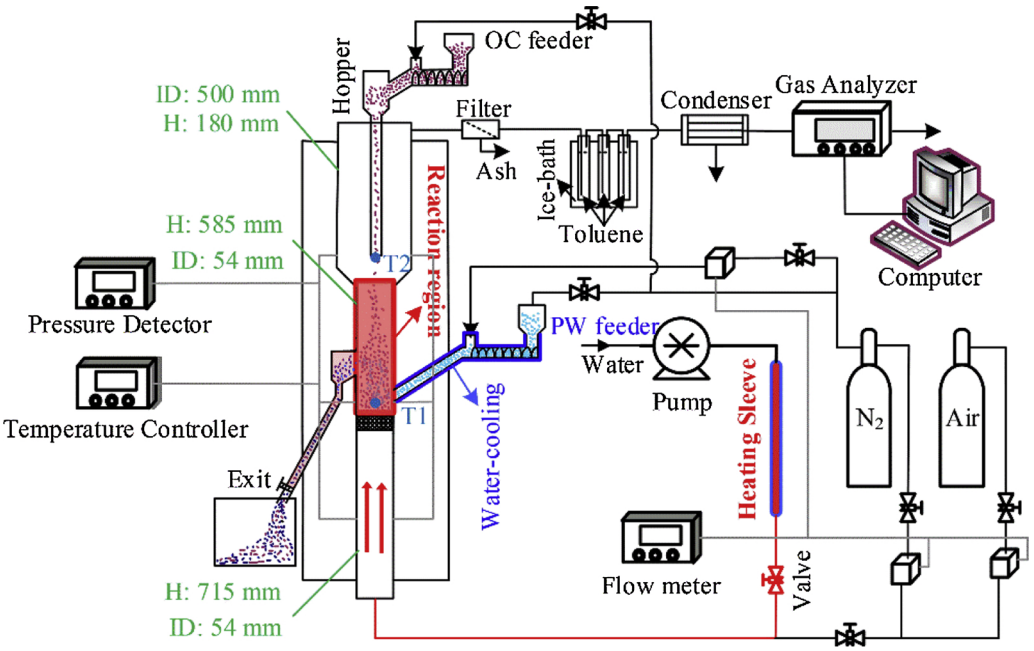

Fig. 11. A schematic view of the semi-continuously operated fluidized bed reactor. (Ma et al., 2019c).

between the oxygen carrier feeding rate and overflow rate were measured and calibrated. For the formal *i*G-CLC tests with plastic waste, an accumulative operation of over 10 h was attained. During the operation, a mixture of 5 vol.% H_2O and 95 vol.% N_2 was used as the fluidization gas, and the thermal power input was 150 W_{th}. The results showed that both the CO_2 yield and carbon conversion could reach nearly 95 %, with the combustion efficiency of 98 % attained at 900 °C. Additionally, the suppressing effect on chlorobenzene formation of the CaO-decorated iron ore oxygen carrier was further demonstrated in the semi-continuously operated fluidized bed reactor, at the expense of slightly decreased activity in comparison to the raw iron ore.

2.3.4.2. Copper ore. Copper ore has been extensively studied as oxygen carrier for CLOU of solid fuels. (Wang et al., 2015; Zhao et al., 2014b) The as-purchased copper ores usually have low Cu content and are not suitable for chemical looping application. Therefore, the original copper ore should go through a sulfidation process, changing copper oxides in the original ore to copper sulfides and hence improving the surface hydrophobicity. To eliminate the sulfur content as well as to improve its physical strength, the received copper ore was first calcined at 500 °C for 5 h and then at 1000 °C for 10 h in an air atmosphere muffle furnace. After calcination, the active phases in the copper ore were 21.04 wt.% CuO and 70.05 wt.% $CuFe_2O_4$. The effects of temperature on the oxygen release (900 − 1000 °C) and oxygen uptake (600 − 950 °C) rates of the copper ore were first studied in a batch fluidized bed reactor. (Zhao et al., 2014b) Generally, both the oxygen release and uptake rates of copper ore increased along with the reaction temperature. Fig. 12 shows the O_2 decoupling characteristic of copper ore at five different temperatures. Two distinct peaks were observed at all temperature conditions, with a small peak occurred during the first 50 s and then followed by a major peak. As indicated by XRD analyses together with the calculated theoretical oxygen capacity of copper ore, the first peak was attributed to the decoupling of CuO and the second peak was resulted from the decoupling of both CuO and $CuFe_2O_4$. Furthermore, CLOU characteristics of the copper ore with GP anthracite were investigated. Several key influencing factors, like reaction temperature, fluidization rate, oxygen carrier to fuel ratio, coal particle size, and steam concentration were systematically evaluated. Under the optimal experimental condition, high combustion efficiency (> 95 %) and CO_2 yield (> 0.96) were attained. Moreover, stable

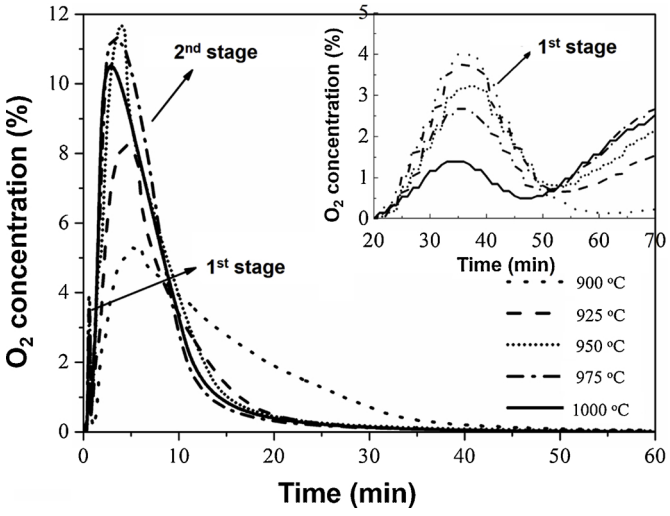

Fig. 12. The O_2 decoupling behavior of copper ore oxygen carrier at different temperatures. (Zhao et al., 2014b).

reactivity of the copper ore oxygen carrier was achieved during the subsequent cyclic redox test.

To further examine the fuel adaptability of copper ore, CLOU tests with three coals of different ranks (GP anthracite, FG bituminous, and SL lignite) were conducted. (Wang et al., 2015) For the three coals, both increasing the reaction temperature and decreasing coal rank were beneficial for carbon conversion. The rate-limiting step in coal-derived CLOU process was found to be the conversion of coal char with low-concentration of O_2 in the case of excessive oxygen carrier, and the limiting effect was more obvious for higher-rank coals. Introducing steam or CO_2 as gasification agent could increase the instantaneous char conversion rate by as much as 50 % for the GP anthracite. Promising as it was, sintering issue still occurred at 950 °C when using SL lignite as fuel.

In addition, copper ore was also applied to CLG of sawdust for syngas production. (Guo et al., 2015) Temperature programmed reaction was first conducted in TGA to investigate the role of oxygen carrier in sawdust pyrolysis process. The presence of copper ore could greatly

enhance the conversion of sawdust when compared to silica sand. In a batch-fluidized bed reactor, effects of different solid materials (copper ore, hematite, or silica sand) on the biomass conversion and gas products distribution were investigated. In comparison to silica sand and hematite, both the biomass conversion and CO_2 production (from side combustion reactions) increased when using copper ore as solid inventory. CO_2 formation degraded the value of the produced syngas to some extent, yet partial full oxidation of syngas in the reforming process can generate *in situ* heat to balance the endothermic reforming reactions therein, which was beneficial for auto-thermal operation. Note that, the tar content decreased significantly in the presence of oxygen carrier, which was 22.15 g/Nm^3 for silica, while were 11.76 g/Nm^3 and 10.18 g/Nm^3 for hematite and copper ore, respectively. These results indicated that copper ore and hematite may catalyze the decomposition of tar and eventually achieve tar reduction in the biomass gasification process.

As noted above, the sintering issue of copper ore limits its application at high temperatures in CLOU. (Wang et al., 2015) In order to increase the sintering-resistance of copper ore, calcium aluminate cement was adopted as inert support *via* the wet mechanical mixing method. (Tian et al., 2015) The cement loading ratio was found to be critical for the performance of the resulted oxygen carrier particle: high cement loading ratio was generally beneficial to attaining high physical strength of the oxygen carrier but would eventually decrease the oxygen capacity and degrade the porous structure by pore blocking. TGA tests with synthesis gas (25 vol.% H_2 + 35 vol.% CO + 40 vol.% CO_2) indicated that 20 wt.% of cement addition was the optimum value. Further batch fluidized bed test with SL lignite as fuel at 950 °C demonstrated the superior reactivity and sintering resistance of the 20 wt.% of cement decorated copper ore oxygen carrier (denoted as Cu-C-20). As shown in Fig. 13, the peak value of the carbon conversion rate attained at the 10th cycle for Cu-C-20 was 0.042 s^{-1}, while it was 0.019 s^{-1} for pure copper ore, at 950 °C. Moreover, the cycled copper ore agglomerated seriously, yet no obvious sintering phenomenon occurred to the Cu-C-20 sample. Preliminary economic analysis on the raw material costs further indicated the feasibility of using cement decorated copper ore as oxygen carrier in the coal-derived CLOU process.

2.3.4.3. Mixed ores. Considering that hematite is cheap and environmentally benign but less active, while copper ore is more active but suffers from sintering and agglomeration issues at high temperature, mechanically mixed copper ore and hematite was thus proposed as binary oxides oxygen carrier. (Yang et al., 2015) Synergistic effect between copper ore and hematite was observed in

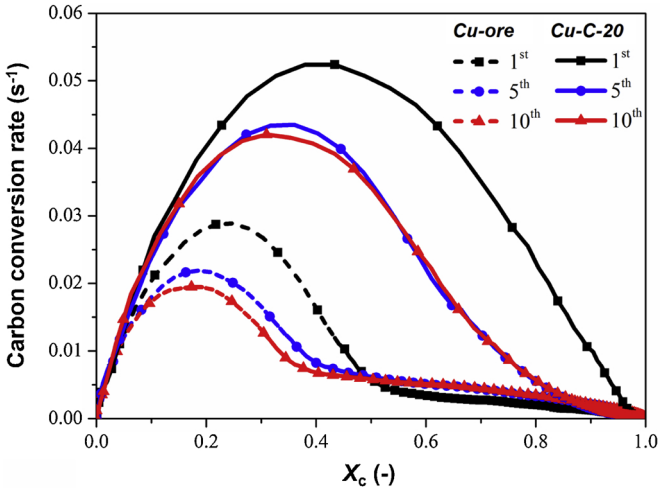

Fig. 13. Carbon conversion rate *vs.* carbon conversion in coal-derived CLOU process with copper ore and Cu-C-20 as oxygen carriers at different cycles. Fuel: SL lignite; temperature: 950 °C. (Tian et al., 2015).

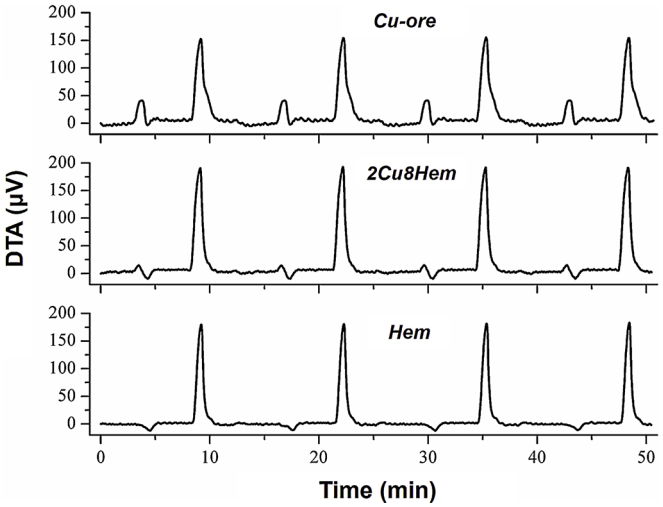

Fig. 14. DTA signals of pure copper ore, pure hematite and 2Cu8Hem oxygen carriers in TGA with synthesis gas as fuel (1 min) and air as oxidizing agent (3 min) during 4 redox cycles. Reaction temperature: 950 °C. (Yang et al., 2015).

TGA tests with synthesis gas (25 vol.% H_2 + 35 vol.% CO + 40 vol.% CO_2) as fuel. The optimum copper ore mixing ratio was attained in the range of 10 – 20 wt.%, based on the consideration of reactivity, stability, and copper ore utilization efficiency. The synergistic effect achieved between copper ore and hematite was explained in two aspects: 1) dispersion of copper ore in hematite alleviated the sintering issue of copper ore at high temperature, thus improved the available oxygen amount of copper ore in reaction; 2) interaction between Fe_2O_3 and CuO led to the formation of $CuFe_2O_4$, which exhibited higher oxygen carrying capacity than that of Fe_2O_3 and CuO with the same mass. Moreover, as shown in Fig. 14, the reaction of synthesis gas with copper ore was exothermic, while it was endothermic with hematite. Thermal neutral was eventually achieved when the copper ore ratio was 20 wt.% in the mixed ore oxygen carrier (denoted as 2Cu8Hem), which was beneficial for auto-thermal operation in the FR.

However, as the copper ore and hematite particles were physically mixed, segregation phenomenon may occur to the particles in fluidized bed reactor due to their different densities. Further improvement of the mixed copper ore and hematite oxygen carrier was realized by using cement as binding medium. (Tian et al., 2017c) Waste fine powders of copper ore and hematite (smaller than 0.1 mm, not fluidizable in the CLC reactor) were reused by cement bonding (20 wt.% of cement loading ratio, as optimized in previous work (Tian et al., 2015)). Different from the physical mixing method used before (Yang et al., 2015), cement binding led to the coexistence of hematite and copper ore in one particle. In this case, particle segregation issue in fluidization was resolved. Consequently, much higher carbon conversion rate was attained when using the same coal (GP anthracite) as fuel under similar reaction condition. Moreover, thermal neutrality was also attained within an oxygen carrier particle when reacting with synthesis gas (simulated coal gasification products).

As it can be seen from Table 5, different types of iron ore and copper ore, foreign ion decorated iron ore, and ore mixtures have been comprehensively investigated for various chemical looping applications. To summarize, the biggest advantage of natural ore material is the low-cost, which is thus highly promising for industrial-scale application.

2.3.5. Other oxygen carriers

As reviewed above, most of the oxygen carriers discussed were Fe- and Cu-based materials developed at HUST. In this section, a brief introduction of several other kinds of oxygen carriers studied by the same

Table 5
Summary of natural ore oxygen carriers for chemical looping.

Material	Active phase (wt.%)	Application	Facility	Reacting agent	Ref.
Hematite	Fe_2O_3 (91.6); Fe_2O_3 (65.9)	*i*G-CLC	b-FB, i-FB	CH_4, Coals, O_2	(Ma et al. 2017a, 2015a,b)
CuO decorated hematite	Fe_2O_3 (81.9), (6% CuO doping)	*i*G-CLC	b-FB	Coals, O_2	(Yang et al., 2014)
CaO decorated hematite	Fe_2O_3 (81.9), (5-15 wt.% CaO doping)	*i*G-CLC	b-FB	Perfusion tube, O_2	(Wang and Zhao, 2016)
CaO decorated hematite	Fe_2O_3 (81.9), (5 wt.% CaO doping)	*i*G-CLC	sc-FB	Perfusion tube, O_2	(Ma et al., 2019c)
Copper ore	CuO (21), $CuFe_2O_4$ (70)	CLOU	b-FB	Coals O_2	(Wang et al., 2015; Zhao et al., 2014b)
Copper ore	CuO (21), $CuFe_2O_4$ (70)	CLR	TGA, b-FB	Pine sawdust, O_2	(Guo et al., 2015)
Cement decorated copper ore	CuO (16.8), $CuFe_2O_4$ (56)	CLOU	TGA, b-FB	Synthesis gas, coal, O_2	(Tian et al., 2015)
Physically mixed copper ore and iron ore	CuO (4.2), Fe_2O_3 (65.6), $CuFe_2O_4$ (14)	CLC	TGA, b-FB	Synthesis gas, coal, O_2	(Yang et al., 2015)
Cement bonded copper ore and hematite	CuO (3.4), Fe_2O_3 (52.5), $CuFe_2O_4$ (11.2)	*i*G-CLC	TGA, b-FB	Synthesis gas, coals, O_2	(Tian et al., 2017c)

Notes: i-FB, inter-connected fluidized bed reactor; sc-FB, semi-continuously operated fluidized bed reactor.

group will be compiled, including Ni-, Mn-, and $CaSO_4$-based materials.

Using $Al(OC_3H_7)_3$ and $Ni(NO_3)_2$ as raw materials, NiO/$NiAl_2O_4$ oxygen carrier was prepared by the sol-gel method. (Zhao et al., 2008a, b) The NiO content, sintering temperature, and sintering time were first optimized by characterizing the resulted NiO/$NiAl_2O_4$ oxygen carrier *via* BET, SEM, and XRD. (Zhao et al., 2008a) The results indicated that the oxygen carrier with 60 wt.% of NiO, at a sintering temperature of 1300 °C and a sintering time of 6 h showed the most promising physicochemical properties. Cyclic tests of the optimized NiO/$NiAl_2O_4$ oxygen carrier with CH_4 in TGA demonstrated its physical and chemical stability under the redox reaction context. Further test of the same NiO/$NiAl_2O_4$ oxygen carrier was conducted in TGA with coal char as fuel. (Zhao et al., 2008b) Temperature programmed reaction results showed that NiO/$NiAl_2O_4$ started to directly react with coal char rapidly when the temperature reached 850 °C. The reactivity stability of the oxygen carrier was further confirmed by cyclic test with H_2. ESEM characterization indicated that porous structure of the cycled sample was well maintained and XRD analysis demonstrated its phase stability.

A thermodynamic simulation was conducted to investigate the sulfur behavior in the CLC process using $CaSO_4$ as oxygen carrier and coal-derived synthesis gas as fuel. (Wang et al., 2011a) It was found that at the low temperature range (100 − 400 °C), the main sulfur species was H_2S. When increased the temperature to a higher range (400 − 915 °C), CaS and CO_2 were generated *via* the reaction between $CaSO_4$ and H_2/CO. Further increase of the reaction temperature to over 915 °C would lead to the decrease of CaS percentage, due to the side reaction between CaS and $CaSO_4$. Considering the low reactivity and sulfur emission from side reactions of $CaSO_4$, a kind of $CaSO_4$-CuO mixed material was prepared *via* the combined template and sol-gel combustion synthesis method. (Wang et al., 2017) The mixed oxygen carrier was found to be able to greatly enhance the activity towards YN lignite in comparison to single $CaSO_4$ or CuO oxygen carrier. DTA analysis of the reaction between YN lignite and $CaSO_4$-CuO oxygen carrier indicated an overall exothermic characteristic, which was beneficial to attaining auto-thermal operation. Moreover, FTIR analysis of the gaseous products and XRD characterization of the solid products showed that the gaseous sulfur species generated from side reactions of $CaSO_4$ were effectively suppressed by Cu_2S formation.

In collaboration with *C.S.I.C.* researchers, four different manganese minerals were tested as oxygen carriers in the CLC process. (Mei et al., 2015b, 2016) XRD results indicated that the main crystalline phases of the calcined manganese minerals were Mn_2O_3, Mn_3O_4, Fe_2O_3, and inert SiO_2. However, Mn_2O_3 cannot be fully regenerated by air after reduction. With this in mind, TGA tests were first conducted to determine the stable phases of the manganese minerals under redox condition. The results indicated that only the redox pairs of Mn_3O_4/MnO and Fe_2O_3/Fe_3O_4 can be utilized under the CLC context, and no obvious CLOU property was observed for all the four manganese minerals. Cyclic test of the manganese minerals in a batch fluidized bed reactor showed a decrease of activity towards CH_4 at the first 10 cycles, but stable reactivity was attained afterwards and well-maintained till the end of the test. Structure change of the used samples was observed, due to the transition of mesopores to macropores inside the particles. (Mei et al., 2015b) The feasibility of applying the above four manganese minerals to coal-derived CLC process was then investigated in a batch fluidized bed reactor. (Mei et al., 2016) When compared with the iron ore tested in continuous CLC units under similar condition, much higher instantaneous char gasification rate was attained for all the manganese minerals, mainly due to the existence of K, Na, and Ca contents which could catalyze the char gasification. For the most reactive manganese mineral, the CO_2 capture efficiency that can be reached in the continuous CLC unit with a carbon stripper system was calculated. The calculation results indicated that 99 % CO_2 capture efficiency could be attained with solid inventory as low as 300 kg/MW_{th} at 1000 °C.

Table 6 gives a brief summary of several other kinds of oxygen carrier that were investigated. As it can be seen, in comparison to Fe- and Cu-based oxygen carriers, these materials have not been extensively studied. Nevertheless, the preliminary results attained indicated that they could be promising oxygen carriers in CLC and deserved further investigation.

2.3.6. Comparison of different oxygen carriers

Table 7 gathers and compares several oxygen carrier representatives for chemical looping processes. As it can be seen, the sol-gel derived

Table 6
Several other kinds of oxygen carrier for chemical looping.

Material	Active phase (wt.%)	Preparation method	Application	Facility	Reacting agent	Ref.
NiO/$NiAl_2O_4$	NiO (60)	SG	CLC	TGA	Coal, CH_4, O_2	(Zhao et al., 2008a, b)
$CaSO_4$-CuO	CaSO4 (60); CuO (40)	SGCS	CLC	TGA	Coal, O_2	(Wang et al., 2017)
Manganese ores	Mn_3O_4 (65.6-71.8); Fe_2O_3 (5.2-18.6)	–	CLC	b-FB	Coal, O_2	(Mei et al., 2015b, 2016)

Table 7
Comparison of different oxygen carriers for various chemical looping applications.

Oxygen carrier	Active phase (wt. %)	Application	Fuel type	Performance	Ref.
Fe_2O_3/Al_2O_3	Fe_2O_3 (60)	*i*G-CLC	Coal	Low solid inventory of 600 kg/MWth to achieve 99% char conversion at 900 °C	(Mei et al., 2014)
$CuO/CuAl_2O_4$	CuO (60) $CuAl_2O_4$ (40)	CLR	Pine sawdust	54.9% increase in carbon conversion and 67% decrease in tar yield in comparison to direct pyrolysis at 800 °C	(Zhao et al., 2015)
$CuO@TiO_2$-Al_2O_3	CuO (77.5)	CLOU	H_2, coal	Coal combustion efficiency between 97.2-98.3% within 20 cycles at 900 °C	(Tian et al., 2017b)
$CuO@TiO_2$-Al_2O_3	CuO (77.5)	CLAS	–	Average O_2 production rate of 3.34×10^{-7} mol O_2/s per gram oxygen carrier at 950 °C during 10 h run	(Tian et al., 2018b)
CuO/Fe_2O_3	CuO (33.3) Fe_2O_3 (66.6)	CLG	Pine sawdust	Gas yield of 1.16 Nm^3/kg and tar yield of 7.5 g/kg compared to 0.76 Nm^3/kg and 14.55 g/kg in thermal blank at 800 °C	(Niu et al., 2018; Tian et al., 2018a)
Hematite	Fe_2O_3 (81.9)	*i*G-CLC	CH_4, coal	81.3% CH_4 conversion (CH_4); above 0.85 CO_2 yield and above 73.5% combustion efficiency (coal)	(Ma et al., 2015a, b)
Copper ore	CuO (21) $CuFe_2O_4$ (70)	CLOU	Coal	High combustion efficiency above 96% and CO_2 yield above 0.95	(Zhao et al., 2014b)
CuO decorated hematite	CuO (6) Fe_2O_3 (77)	*i*G-CLC	Coals	CO_2 yield of 0.94 for SH and 0.98 for GP	(Yang et al., 2014)
Physically mixed copper ore and hematite	CuO (4.2) Fe_2O_3 (65.6) $CuFe_2O_4$ (14)	CLC	Syngas, coal	Average reduction rate of 0.77×10^{-3} s^{-1} with syngas; 0.79 CO_2 yield with GP	(Yang et al., 2015)
Cement bonded copper ore and hematite	CuO (3.4) Fe_2O_3 (52.5) $CuFe_2O_4$ (11.2)	*i*G-CLC	Syngas, coals	CO_2 yield of over 0.94; maximum carbon conversion rate of 0.024 s^{-1} with lignite	(Tian et al., 2017c)

Fe_2O_3/Al_2O_3 oxygen carrier was highly reactive for *i*G-CLC of lignite (Mei et al., 2014), which showed much higher char gasification rate in comparison to several other Fe-based materials. (Abad et al., 2012b; Jerndal et al., 2011; Leion et al., 2007) Calculation results based on the reaction data attained in batch fluidized bed tests indicated typical low solid inventory (600 kg/MWth) for the sol-gel derived Fe_2O_3/Al_2O_3 oxygen carrier to achieve 99 % char conversion at 900 °C. Chemical looping auto-thermal gasification/reforming of biomass was demonstrated by the $CuO/CuAl_2O_4$ oxygen carrier. (Zhao et al., 2015) Biomass gasification/reforming tests in a batch fluidized bed reactor showed a high carbon conversion of 95.6 % and low tar yield of 7.29 g/Nm^3 for this oxygen carrier in comparison to 62.3 % carbon conversion and 22.15 g/Nm^3 tar yield attained in thermal blank. Synergistic reactivity was observed for the bimetallic CuO/Fe_2O_3 oxygen carrier in CLG of pine sawdust (Niu et al., 2018; Tian et al., 2018a), which showed a significant increase in syngas yield when compared with thermal blank as well as pure CuO or Fe_2O_3 oxygen carrier. The Cu content was found to be beneficial for the decomposition of small molecular compounds while the Fe content could decrease the formation of large molecular compounds in tar. The hierarchically structured $CuO@TiO_2$-Al_2O_3 oxygen carrier prepared by the SATCS method exhibited both high activity and superior physicochemical stability in the CLOU and CLAS processes. (Tian et al., 2017b, 2018b) For the reaction of $CuO@TiO_2$-Al_2O_3 with coal in a batch fluidized bed reactor, combustion efficiency was maintained at around 97.8 % at 900 °C during 20 cycles. Continuous O_2/CO_2 stream production in a paralleled fluidized bed reactor was also demonstrated by applying this oxygen carrier to the CLAS process. During 10 h of continuous running at 950 °C, an average O_2 production rate of 3.34×10^{-7} mol O_2/s per gram oxygen carrier was attained.

For the copper ore and iron ore, reactivity promotion was achieved *via* foreign ions introduction or using ore mixtures. Copper decoration (6 wt.% CuO) of hematite was found to increase the coal combustion efficiency by 7.5 percentage points in comparison to pure hematite in the *i*G-CLC process at 900 °C. Inward diffusion of Cu cation into the particle was observed for the cycled oxygen carriers *via* SEM-EDX analysis, which was beneficial to the oxygen carrier from the standpoint of sintering resistance. (Yang et al., 2014) Cement bonded fine hematite and copper ore particles was proved to be a promising way for fine ore powders reutilization. (Tian et al., 2017c) Synergistic reactivity between copper ore and iron ore was greatly improved after cement addition in comparison to physically mixed copper ore and iron ore. (Yang et al., 2015) Moreover, the cement content could help to attain high sintering resistance of the resulted oxygen carrier, at much lower cost than traditional inert supports. (Tian et al., 2015)

Although a wide variety of OCs have been assessed by us as well as numerous colleagues, there are at least two issues that need to be resolved urgently. The first issue is to acquire sufficient cheap, environmentally friendly, durable, and reactive (as highly as possible) OC particles. Natural ore or industrial waste (*i.e.*, red mud) can meet these requirements except for reactivity. A composite of varied ores or wastes (*e.g.*, physically mixed iron ore and copper ore, cement bonded fine hematite and copper ore particle) could attain higher reactivity and better overall performance. Large-scale preparation of these OC particles (from chemical reagent, or natural ore, or industrial waste, or hybrid) is of uppermost priority. The second issue is to achieve optimal matching between various oxygen carriers and multifarious fuels (especially solid fuels) for gaining the compromise between cost and efficiency of the chemical looping process. This is because one oxygen carrier may perform well only for limited fuels. For example, the iron-based OC will suit for the easily-gasified lignite, biomass or plastic waste to attain quite high combustion efficiency. Copper-based OC, on the other hand, as an oxygen uncoupling material (although more expensive than the iron-based OC) may be advantageous on the whole when combusting the difficultly-gasified anthracite or petroleum coke. Nevertheless, this issue becomes more complicated when a variety of reaction mode and reactor configuration are considered. This is because the chemical looping performance of a specific fuel using a specific OC will undoubtedly be dependent on reaction atmosphere.

2.4. Microcosmic-level understanding and rational synthesis of oxygen carrier

Previously, investigations on the performance of oxygen carrier in chemical looping processes were mainly conducted by experiments. Generally, after the synthesis of the oxygen carrier, TGA or fluidized bed reactor tests would be conducted to evaluate its reactivity and redox stability, either with gaseous fuels or solid fuels. Then, physicochemical characterizations would be used to illustrate the possible changes, *e.g.*, crystalline phase, surface morphology, of the oxygen carrier before and after reaction. The “trial and error” method has been the main research route for the development of oxygen carriers in

literatures. Even though this method was widely adopted, it was blind to some extent, which was not capable for the rational design of oxygen carrier. In Section 2.3.2, the synthesis and applications of the $CuO@TiO_2$-Al_2O_3 oxygen carrier in different chemical looping processes has been briefly introduced. In this section, we highlighted the rational design of $CuO@TiO_2$-Al_2O_3 oxygen carrier, step by step, which demonstrated how to effectively design an oxygen carrier with desirable properties from the bottom up.

The rational design of Cu-based oxygen carrier was started with an in-depth understanding of the influencing factors on the oxygen decoupling property as well as the interactions between active phase and inert support. DFT calculation was conducted to investigate the oxygen decoupling mechanism of Cu-based oxygen carriers as well as the effect of inert supports, at an atomic and molecular level. (Zhang et al., 2015; Zhao et al., 2017) The main objective of conducting DFT calculations was trying to reveal the basic factors that affected the sintering resistance and activity of the oxygen carrier: a higher adsorption energy of CuO on the support is beneficial to sintering resistance, and a lower energy barrier of the oxygen decoupling process favors the oxygen carrier activity.

The most probable oxygen decoupling pathways of CuO (1 1 1) surface at different stages, *i.e.*, O_2 formation, O_2 desorption, and O anion diffusion in slab, were investigated. (Zhang et al., 2015) As schematically shown in Fig. 15, the formation (S1) and desorption (S2) of O_2 created O vacancies at the CuO surface, which facilitated the migration of the O onion from the subsurface to the surface (S3). DFT calculation results indicated that the O_2 formation and O_2 desorption steps were the rate-limiting steps for the oxygen release of CuO, with the energy barriers of 3.0 eV and 2.7 eV, respectively. This was further verified by CuO decoupling experiments in TGA. As known, $CuAl_2O_4$ can also release gaseous O_2 at high temperature. But different from CuO, the O anion diffusion step was significantly endothermic for the decomposition of $CuAl_2O_4$, with an energy barrier of 2.53 eV (compared to 0.88 eV for CuO), indicating that all the three steps are rate-limiting for the decoupling of $CuAl_2O_4$. Therefore, much higher temperature was required for the $CuAl_2O_4$ decomposition than that of CuO, as also supported by TGA results.

The effects of $CuAl_2O_4$ support on the reactivity and sintering resistance of CuO were also investigated. It was found that the Al sites at the surface of $CuAl_2O_4$ were critical to suppress the sintering of CuO. To be more specific, the adsorption energies of the Cu_4O_4 nanoclusters at the surface of $CuAl_2O_4$ and pure CuO were -4.25 eV and -2.92 eV, respectively, which explained the high sintering resistance of the CuO/$CuAl_2O_4$ oxygen carrier. The influence of $CuAl_2O_4$ support on the activity of CuO was also significant. Due to the electron redistribution within the CuO nanocluster (caused by the support), the O_2 desorption step turned to be the only rate-limiting step for the CuO/$CuAl_2O_4$ system. Even though such electron redistribution was not good for the activity of CuO, suitable content of $CuAl_2O_4$ support was still necessary to prevent CuO sintering.

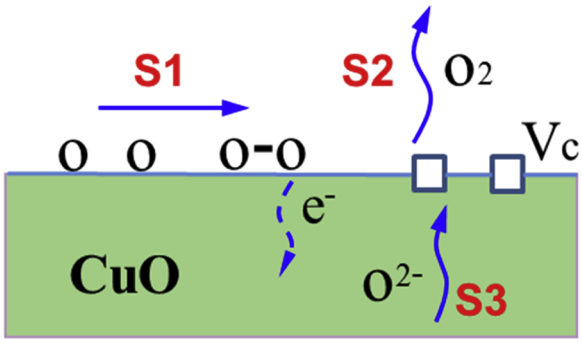

Fig. 15. Oxygen release mechanism of CuO. Arrows indicate the moving direction of different species. (Zhang et al., 2015).

As indicated by DFT calculation results, the introduction of inert support was not conducive to the oxygen release of CuO. Among the four commonly used inert supports in literatures, *i.e.*, TiO_2, ZrO_2, $CuAl_2O_4$, and $MgAl_2O_4$, TiO_2 was found to exert the minimum negative effect on the oxygen decoupling performance of CuO. (Zhao et al., 2017) Nevertheless, TiO_2 showed inferior sintering resistance when compared with the other three inert supports. The particle sintering process is essentially solid-state diffusion driven by the decrease of grain surface energy. Detailed understanding of the sintering mechanism of CuO nanograins within the particle, as well as the interactions between CuO and inert support materials (TiO_2, ZrO_2, and SiO_2) were also revealed by molecular dynamics (MD) simulation. (Zhao et al., 2018) It was found that the pure CuO nanograin with smaller diameter or at higher temperature tended to be more amorphous. The neck growth between two CuO nanograins was the joint effect of surface diffusion and grain boundary diffusion. Among the three composites oxygen carriers (CuO supported by TiO_2, ZrO_2, or SiO_2), the highest sintering resistance was attained by CuO/ZrO_2.

Moreover, the sintering resistance of CuO can be regulated by adjusting the particle size of inert support. To theoretically understand the sintering behavior of CuO, Zener pinning theory was adopted to study the CuO grain radius growth kinetics at high temperatures. According to the Zener pinning theory, the largest CuO grain radius (R_{max}) during the CuO sintering process is proportional to the support particle size (r), and inversely proportional to the fraction of support material (f). (Xu et al., 2015) In this sense, small support particle size can inhibit CuO grain growth, thus suppress CuO sintering. Therefore, nano TiO_2 particle was selected as support for CuO. However, nm-TiO_2 is much more expensive when compared with the commonly used inert support, like Al_2O_3. While on the other hand, chemical reaction between Al_2O_3 and CuO at high temperature (forming $CuAl_2O_4$ spinel) would degrade the oxygen carrying capacity of the oxygen carrier to some extent. With this in mind, a composite material with hierarchical structure as inert support was proposed, where nm-TiO_2 in the outer layer was used as minor support and cheap μm-Al_2O_3 in the inner layer as main support.

Note that, the nm-TiO_2 particles were prepared by flame synthesis method in lab. Fig. 16 shows a schematic view of the gas flame synthesis facility. N_2 (carrier gas), $TiCl_4$ vapor (TiO_2 precursor), CH_4 (fuel gas), and O_2 (oxidant) were feed into a four-concentric tube burner, from center to the outside. The co-flow diffusion CH_4 flame created a controllable and stable high-temperature region for the synthesis of nm-TiO_2. The nm-TiO_2 products with different proportions of anatase phase and rutile phase were customizable, and particles in a size range of 10 − 50 nm were attained.

Self-assembly template combustion synthesis method was adopted

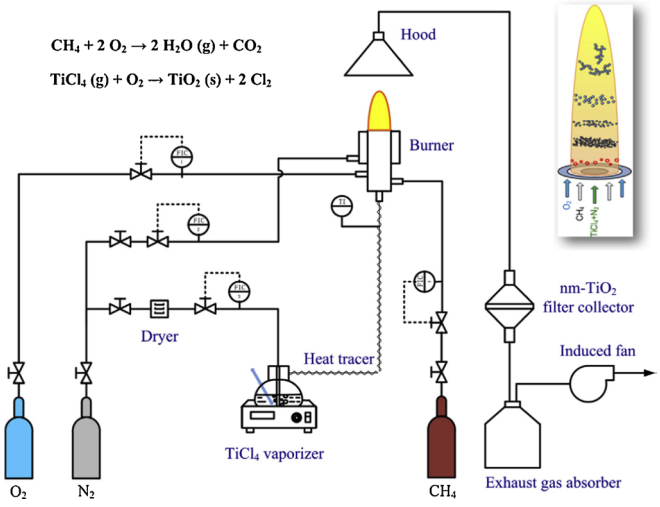

Fig. 16. Flame synthesis of rutile nm-TiO_2. (Xu et al., 2015).

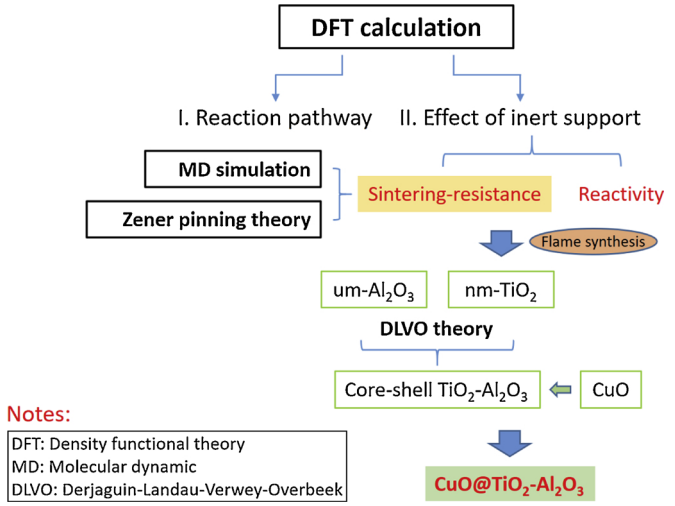

Fig. 17. Rational design route of the $CuO@TiO_2$-Al_2O_3 oxygen carrier.

to obtain the $CuO@TiO_2$-Al_2O_3 oxygen carrier with hierarchical structure. The challenge here was how to effectively and homogeneously coat nm-TiO_2 onto the surface of μm-Al_2O_3. According to the Derjaguin-Landau-Verwey-Overbeek (DLVO) theory, the thermodynamic interactions between two particles in suspension liquid mainly include van der Waals attractive and electric double layer repulsive (or attractive) potentials. By adjusting the pH value of the suspension liquid, the zeta potential of particles can be regulated. It was found that when the pH value was 6, the zeta potential difference between nm-TiO_2 and μm-Al_2O_3 reached the largest. At this point, TiO_2 nanoparticles can coat on the surface of Al_2O_3 spontaneously and uniformly, attaining the hierarchical structure. The Cu-based oxygen carrier with the proposed Al_2O_3-TiO_2 support have been extensively tested in chemical looping processes, which proved to have both high activity and high sintering resistance.

Fig. 17 summarizes the rational design route of the $CuO@TiO_2$-Al_2O_3 oxygen carrier. As can be seen, DFT calculation was employed to reveal the reaction pathway and effect of inert support, MD simulation was adopted to investigate the sintering mechanism of CuO nanograins, and the Zener pinning theory was used to optimize the particle size of inert support. Then, nm-TiO_2 was prepared by flame synthesis method and core-shell TiO_2-Al_2O_3 template was attained in light of DLVO theory. Finally, $CuO@TiO_2$-Al_2O_3 oxygen carrier with hierarchical structure was produced.

Following the rational synthesis route and corresponding self-assembly template synthesis method, a core-shell CaO-based sorbent, *i.e.*, CaO/TiO_2-Al_2O_3, was also prepared, for utilization in the calcium looping process. (Peng et al., 2015, 2016) The cyclic CO_2 capture performance of CaO/TiO_2-Al_2O_3 was systematically investigated *via* both TGA and batch fluidized bed tests. TGA results indicated that much higher CO_2 capture capacity was attained by CaO/TiO_2-Al_2O_3 (0.44 g/g, after 104 cycles) than those of pure CaO (0.35 g/g, after 30 cycles) and CaO/Al_2O_3 (0.27 g/g, after 30 cycles) under severe calcination condition. (Peng et al., 2015) Batch fluidized bed tests also demonstrated that the CO_2 capture capacity of CaO/TiO_2-Al_2O_3 was 50.1 % and 77.3 % higher than those of CaO/Al_2O_3 and CaO, respectively, after 10 carbonation/calcination cycles. (Peng et al., 2016) In addition, a kind of CaO-CuO/MgO@Al_2O_3 material prepared by the self-assembly template synthesis method was adopted for application in calcium looping integrated with CLC (CaL-CLC), hoping to resolve the unstable reactivity of CaO and heat requirement of $CaCO_3$ calcination in calcium looping. (Ma et al., 2019a) For the CaO-CuO/MgO@Al_2O_3 material, rather stable CO_2 uptake capacity of 0.08 g CO_2/g material was attained during 30 cycles in TGA, and thermal neutrality was finally achieved when using CH_4 as fuel in the calcination-reduction step. All these results suggested the superiority of the self-assembly template synthesis method in the preparation of CaO-based sorbents.

In summary, we demonstrated here how to rationally design a hierarchically structured oxygen carrier or sorbent, based on theoretical and microcosmic level understandings, which was hopefully to give insights into the development of potential routes for the synthesis of oxygen carrier with desired physicochemical properties.

2.5. Reaction kinetics

Comprehensive understandings of the reaction kinetics of oxygen carriers in chemical looping processes are essential for the design and modeling of the whole reaction system. Generally, the reactions related to oxygen carriers in chemical looping processes can be treated as non-catalytic gas-solid reactions. Up to date, plenty of kinetics investigations on oxygen carriers have been conducted, using different gas-solid reaction models. (Abad et al., 2007a; Chuang et al., 2009; García-Labiano et al., 2004; Goldstein and Mitchell, 2011; Song et al., 2013; Zafar et al., 2007) The most commonly used kinetics models were the shrinking core model (Ishida et al., 1996; Son and Kim, 2006), nucleation and nuclei growth model (Hossain and de Lasa, 2010; Wang et al., 2013b), and changing grain size model. (Abad et al., 2011; García-Labiano et al., 2005) In the following part, the reaction kinetics of oxygen carriers conducted under the context of CLOU and CLC will be reviewed.

As an early work, reduction kinetics of the sol-gel derived Fe_2O_3/Al_2O_3 oxygen carrier with H_2 was studied *via* the non-isothermal kinetics analysis method. (Zhao et al., 2014a) The experiments were conducted in a chemisorption analyzer, with the temperature ramped from ambient to 1000 °C at a heating rate of 3 − 21 °C/min. It was found that the reduction of Fe_2O_3/Al_2O_3 had two different reaction stages. For the first stage, Fe_2O_3 was reduced to Fe_3O_4, which could be described by the chemical reaction model, $G(X) = (1 - X)^{-1} - 1$, indicating that the reaction between H_2 and Fe_2O_3 was controlled by the surface reaction process. The corresponding activation energy and pre-exponential factor were determined as 125.4 kJ/mol and 16.3 s^{-1}, respectively. For the second stage, Fe_3O_4/Al_2O_3 was further reduced to $FeAl_2O_4$ in nucleation and nuclei growth mode, with the kinetics function of$G(X) = [-\ln(1 - X)]^{3/4}$. The activation energy and pre-exponential factor for the second stage were attained as 87.1 kJ/mol and 15.3 s^{-1}, respectively. A more recent work was conducted to investigate the reduction kinetics of the same Fe_2O_3/Al_2O_3 oxygen carrier with CO, and only the first reduction stage was considered. (Mei et al., 2018) Non-isothermal tests were conducted in TGA, with different heating rates (β = 3 − 20 K/min) investigated, and the peak temperature was 1273 K. Note that, for the kinetics analysis, only the experimental data within the temperature range of 673 − 773 K was used, since thermodynamic calculation results indicated that carbon deposition would occur and affect the kinetics analysis at higher temperatures. Eventually, a 3D nucleation and nuclei growth model, $G(X) = [-\ln(1 - X)]^{1/3}$, was found to best fit the first half reduction stage ($0 < X \leq 0.5$), and the activation energy of 270 kJ/mol and pre-exponential factor of $1.6 \cdot 10^{12}$ s^{-1} were determined. Following that, diffusion effects dominated the second half reduction stage ($0.5 < X \leq 1$). A 2D diffusion model, $G(X) = (1 - X) \cdot \ln(1 - X) + X$, was found to describe well this reaction stage, and the activation energy and pre-exponential factor were attained as 131 kJ/mol and $3.1 \cdot 10^3$ s^{-1}, respectively.

Global reaction kinetics of Fe-Al and Cu-Fe oxygen carriers with coal were also investigated. (Wang et al., 2016b, 2011b,c, 2013a) A recent work was conducted to understand the reaction mechanism between bituminous coal and $CuFe_2O_4$ oxygen carrier from the viewpoint of coal structure and reactivity. (Wang et al., 2016b) The results showed that the oxidation of C—C/C—H groups was the rate-limiting step in the whole coal conversion process, which could achieve the maximum conversion efficiency when the oxygen to fuel ratio was 1.0.

Meanwhile, the transformation path of these groups was also revealed.

Foreign ions introduction was a commonly used method for reactivity promotion of oxygen carrier. (Bao et al., 2013a, b; Ge et al., 2015; Gu et al., 2012) The effect of CaO, K_2O, and Na_2O decoration on the reaction performance of Fe_2O_3/Al_2O_3 oxygen carrier with synthesis gas was investigated. (Wang and Zhao, 2015) Isothermal tests within the temperature range of 850 − 925 °C were conducted in TGA. TGA results showed that the weight loss curves of the three promoted oxygen carriers were similar to those of the raw Fe_2O_3/Al_2O_3 material, but the "tail" at the later stage of the reaction was more obvious for the decorated oxygen carriers, which might be due to the inhibition of lattice oxygen transport by the alkali (earth) metal decoration. Kinetics analysis showed that the reduction of the four samples could be described by the 3D-nucleation and growth model and the largest activation energy was attained for the CaO decorated Fe_2O_3/Al_2O_3 oxygen carrier.

For the operation of large-scale CLC reactors, natural ores were usually used as oxygen carriers due to the low cost and abundant reserves. (Ma et al., 2018a, 2015a, b) In order to better understand the operation of the CLC reactor and conduct computational fluid dynamics (CFD) simulation, the reduction kinetics of the tested hematite was studied in details. (Su et al., 2017a, b) Pre-experiments in TGA were first carried out to eliminate the influence of gas diffusion in the crucible and between the layers of the sample, by adjusting the sample weight, particle size, and gas flow rate. Then, formal tests were performed in the temperature range of 850 − 1000 °C and CO concentration of 5 − 20 vol.%. It was found that the first reduction stage, $Fe_2O_3 \rightarrow Fe_3O_4$, was controlled by gas diffusion in the particle boundary layer, while the second stage ($Fe_3O_4 \rightarrow FeO$) could be described by the surface reaction-controlled shrinking core model. The activation energy for the second reduction stage was determined as 110.8 kJ/mol. The attained kinetics model was further validated by testing in a batch fluidized bed reactor. Under the premise of using logarithmic mean CO concentration at the inlet and outlet, the kinetics model obtained from TGA could describe well the reaction process in the batch fluidized bed reactor.

With regard to Cu-based oxygen carriers, the oxygen release characteristic of the sol-gel derived $CuO/CuAl_2O_4$ oxygen carriers was first investigated in a fluidized bed reactor in CO_2 atmosphere, and comparisons were made with those of $Co_3O_4/CoAl_2O_4$ and Mn_2O_3/Al_2O_3. (Mei et al., 2013a) The mechanism function, activation energy, and pre-exponential factor for the oxygen release process were obtained. It was found that both the CuO and $CuAl_2O_4$ in the $CuO/CuAl_2O_4$ system were active phases during the oxygen release process, and they were reduced to Cu_2O and $CuAlO_2$, respectively. However, for the $Co_3O_4/CoAl_2O_4$ and Mn_2O_3/Al_2O_3 systems, only Co_3O_4 and Mn_2O_3 were the active phase, respectively. The oxygen release processes could all be described by the nucleation and nuclei growth model, but the corresponding mechanism functions were different. The oxygen release process of $CuO/CuAl_2O_4$ oxygen carrier could be described by $G(X) = [-\ln(1 - X)]^{2/3}$, and the corresponding activation energy and pre-exponential factor were 226.37 kJ/mol and 2.99×10^6 s^{-1}, respectively.

The reduction kinetics of the $CuO/CuAl_2O_4$ oxygen carrier was then tested on TGA and the applicability of the obtained kinetics parameters to the batch fluidized bed reactor was analyzed. (Guo et al., 2016) TGA results indicated that the oxygen release process of the oxygen carrier conformed to the Avrami-Erofeev nucleation and nuclei growth model. The corresponding mechanism function was $f(X) = 3/2(1 - X)[-\ln(1 - X)]^{1/3}$, and the activation energy was 343.7 kJ/mol. The solid fuel in the fluidized bed reactor reacted with the O_2 released from the oxygen carrier and generated *in situ* heat, resulted in the increase of reaction temperature, so as to enhance the oxygen release process. Based on the O_2 concentration and temperature correction in the batch fluidized bed reactor, it was found that the kinetics model attained from TGA could describe the CLOU process in the batch fluidized bed well.

Nevertheless, the kinetics parameters attained from above investigations were all apparent data. In other words, these data would be useful at some degree, but they could be temperature-, atmosphere-, and equipment-dependent, which have no universality. To obtain more general kinetics parameters, it is necessary to study the intrinsic reaction kinetics. (Su et al., 2017b) The intrinsic reduction kinetics of hematite with CO was thus investigated. First of all, the suitable reaction temperature range was determined to be 400 − 650 °C by temperature programmed reduction experiment in TGA. Formal tests were then conducted in the batch fluidized bed reactor. By comparing the attained reaction rate with the calculated value under the boundary layer diffusion control condition, it was confirmed that the reduction process was not affected by external diffusion. Thiele modulus and diffusion effective factor were used to analyze the influence of internal diffusion and to fit the intrinsic kinetics parameters. The intrinsic activation energy of the global surface reaction was attained as 74.48 kJ/mol. Moreover, application of the obtained intrinsic kinetics to actual CFD simulation was also discussed.

For the oxygen uptake process of the reduced (after O_2 decoupling) Cu-based oxygen carrier, the reaction kinetics were also studied in TGA, using the core-shell structured $CuO@TiO_2$-Al_2O_3 as oxygen carrier. (Su et al., 2019) The experiments were carried out at the low temperature range (540 − 600 °C), and the effect of internal and external diffusion could be neglected. A mathematical model with two steps, *i.e.*, surface reaction and ion diffusion, was constructed. Two unknown rate constants in the model were globally fitted by a simulated annealing algorithm. The activation energy of the surface reaction step was determined as 50.5 kJ/mol and that of the ion diffusion step was 79.2 kJ/mol. From this kinetic model, it was clear that the oxygen carrier grain was oxidized layer by layer in the oxygen uptake process. Based on DFT calculations, the microscopic mechanism of Cu_2O oxidation can be expressed as in Fig. 18. As also noted, the influence of the gas diffusion should be considered at higher temperatures, and the intrinsic oxidation process in the real CLOU process may be more easily controlled by the surface reaction step, as the activation energy of the ion diffusion step was greater than that of the surface reaction. In this sense, this study "bridges" the microscopic mechanism and microscopic kinetics, being ready for exploring various oxidation/reduction mechanism and kinetics involved in chemical looping processes. We also note here the particle-resolved simulation is beneficial to figure out the complex relationships among chemical reaction, gas (reactant and product) diffusion, and heat transfer occurring at the gas-solid interface, which are pivotal to establish mesoscale models for macroscopic simulation.

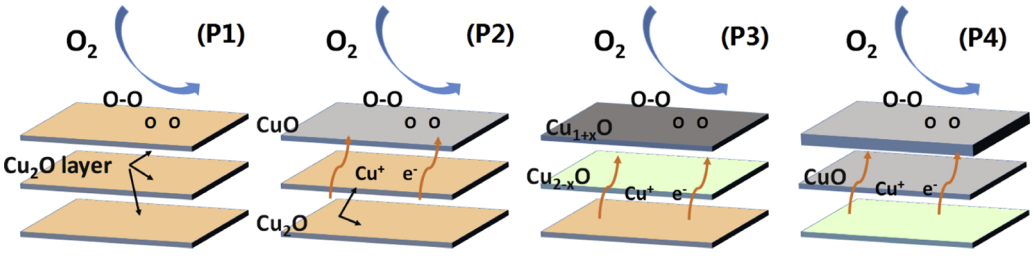

Fig. 18. Schematic view of the Cu_2O oxidation mechanism. (Su et al., 2019).

2.6. The negative effect of sulfur on oxygen carrier

The sulfur compounds in fuels can be detrimental from both environmental and economical standpoints in chemical looping processes. On the one hand, the evolution of SO_2 in the AR and FR will pollute the atmosphere and degrade the purity of the captured CO_2, respectively. On the other hand, the sulfur compounds may react with the active phase to form metal sulfides and/or sulfates and thus poison the oxygen carrier, leading to the inferior activity. Additionally, the low melting point of sulfates, *e.g.*, 805 °C for $CuSO_4$, may easily lead to oxygen carrier agglomeration and affect the solid circulation within the reactor. (Adánez-Rubio et al., 2014)

The effects of H_2S-containing synthesis gas on five commonly used oxygen carriers, *i.e.*, NiO, CuO, Fe_2O_3, Mn_3O_4, and CoO, were thermodynamically investigated. (Wang et al., 2008) Sensitivity analysis indicated that the FR temperature was the main influencing factor for carbon deposition and sulfur evolution. Generally, a higher FR temperature would lead to significant decrease of carbon deposition and enhance the conversion of sulfur compounds into SO_2. The presence of CO_2 and H_2O in the reaction atmosphere was found to be beneficial to inhibiting carbon deposition.

An experimental and thermodynamic study on the sulfur fate in CLC of H_2S-containing synthesis gas (4000 ppm H_2S, 25 % H_2, 35 % CO, and 39.6 % CO_2) using copper ore as oxygen carrier was conducted. (Wang et al., 2016c) As indicated by TG results (as shown in Fig. 19), a weight gain occurred in the test with H_2S-containing synthesis gas, but not for the test with H_2S-free synthesis gas. The weight increase at the end of the reduction stage was attributed to the sulfidation reactions between sulfur compounds and copper ore oxygen carrier. HSC simulation results showed that the main metal sulfides were Cu_2S and FeS, and copper oxides were more reactive towards H_2S than that of iron oxides. Additionally, high reaction temperature was found to be favorable for the generation of SO_2, while lower temperature was beneficial to forming iron sulfides. TG-FTIR results demonstrated that SO_2, COS, and CS_2 were the main gaseous sulfur species generated. The existence of H_2S in fuel gas was found to degrade both the oxygen carrying capacity and reactivity of the copper ore oxygen carrier in batch fluidized bed tests. XRD analysis confirmed the formation of sulfide products, *i.e.*, Cu_2S and FeS.

The sulfur fate in CLOU of high-sulfur coal (SC coal) using the same batch of copper ore oxygen carrier was further studied, and a kind of low-sulfur coal (GP coal) was also tested for comparison. (Tian et al., 2017a) Two SO_2 peaks were observed for both SC and GP coals during the CLOU process, yet the peak intensity for the two coals were

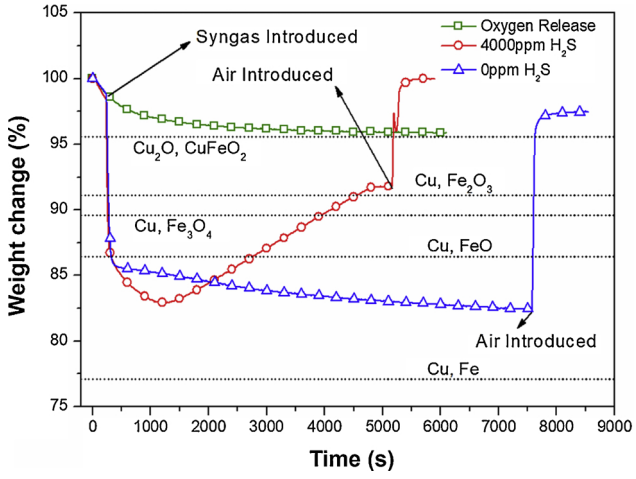

Fig. 19. TG curve for the reduction and regeneration of copper ore under different reduction atmospheres at 900 °C. Fuel: synthesis gas with or without 4000 ppm H_2S. (Wang et al., 2016c).

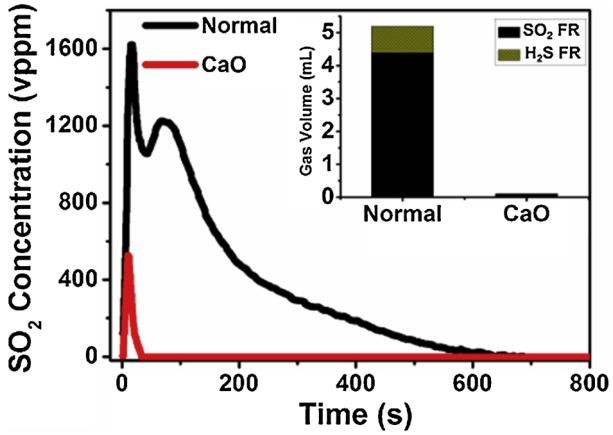

Fig. 20. Effect of CaO addition on the SO_2 evolution behavior in coal-derived CLOU process. Fuel: SC coal; reaction temperature: 900 °C. (Tian et al., 2017a).

different. The two distinct SO_2 peaks were explained to result from the volatiles combustion and coal char combustion, respectively. For the test with SC coal, most of the sulfurous gases were released during the reduction step. The majority of the gaseous sulfur compounds were in the form of SO_2 and only a small proportion of H_2S was detected. CaO addition was found to be effective for SO_2 removal in the CLOU process. As shown in Fig. 20, after the introduction of CaO, only one small SO_2 peak was observed at the beginning of the reaction, and the desulfurization efficiency was attained as high as 98 %.

Generally, Cu-based oxygen carriers are sensitive to sulfur compounds, while Fe-based materials are highly sulfur-resistant (de Diego et al., 2014). Moreover, due to the two relatively independent reaction stages (volatiles conversion stage and coal char conversion stage) of coal in *i*G-CLC, the sulfur evolution characteristics were different accordingly. (Tian et al., 2017a) Therefore, a two-stage micro-fluidized bed reactor, was used to separately investigate the sulfur fate in coal pyrolysis and coal char gasification processes, using a sol-gel derived Fe_2O_3/Al_2O_3 as oxygen carrier and a typical Chinese lignite as fuel. (Ma et al., 2018b; Wang et al., 2018) As shown in Fig. 21, by loading coal and oxygen carrier samples separately in the two-stage reactor, *in situ* coal pyrolysis products could be generated and the influence of oxygen carrier on the coal pyrolysis process was thus eliminated. In comparison to the blank test (loaded with silica sand instead of Fe_2O_3/Al_2O_3 oxygen carrier in the second reactor), the sulfur species distribution changed significantly when the pyrolysis products were introduced upon oxygen carrier, which changed from 70.1 % H_2S, 0.2 % SO_2, 0.8 % COS, and 13.1 % CS_2 to 26.0 %, 68.2 %, 0 %, and 0 %, respectively. HSC simulation results indicated that most of the H_2S could be converted to SO_2

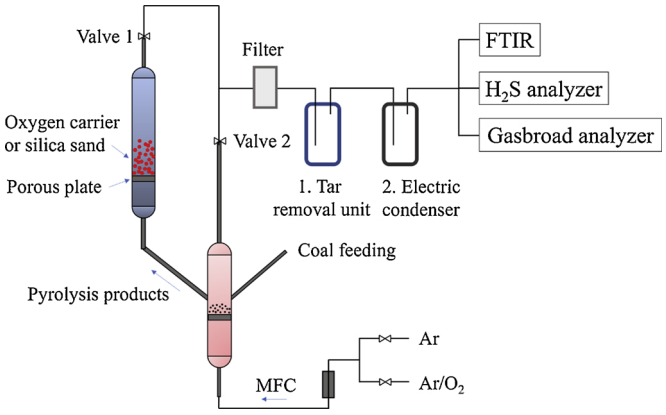

Fig. 21. A schematic view of the two-stage fluidized bed reactor. (Ma et al., 2018b).

via the reaction $H_2S + 9Fe_2O_3 \rightarrow Fe_3O_4 + H_2O + SO_2$. While in the coal char conversion stage (char was converted *via* the *i*G-CLC reaction mode, with CO_2 as gasification agent), SO_2 was almost the sole gaseous sulfur product. Increased the reaction temperature was found to exert more significant impact on the sulfur evolution in the char gasification process than that in the coal pyrolysis process, which was similar to the effect of temperature on the carbon conversion process. Moreover, solid phase sulfur was not detected at the surface of the oxygen carrier, which mainly existed in the form of $CaSO_4$ in coal ash.

For the bimetallic $CuFe_2O_4$ oxygen carrier, insights into the migration and redistribution of sulfur species in CLC of a Chinese coal (LZ coal) was explored by TGA together with several physicochemical characterization techniques. (Wang et al., 2016a) Gaseous FTIR spectroscopy and XPS analysis revealed that SO_2 were mainly generated from the oxidation of H_2S by $CuFe_2O_4$ during the coal pyrolysis stage. Thermodynamic simulation results showed that the oxygen to fuel ratio was the most important factor to affect the migration and conversion of sulfur compounds in coal.

In addition to the sulfur, the fate of mercury during *i*G-CLC of coal was also investigated schematically. Mercury distribution within two elementary sub-processes (coal pyrolysis and char gasification) were experimentally identified. It was found that the release rate and amount of mercury is nearly irrelevant to the presence of OC (here hematite), however the OC will promote the conversion of $Hg^0(g)$ to $Hg^{2+}(g)$, which is potentially beneficial for mercury removal *via*, *e.g.*, wet-FGD (flue gas desulfurization) or wet-ESP (electrostatic precipitator).

3. Development of CLC reactors

For the successful implementation of CLC, as mentioned above, one critical aspect is the selection of oxygen carrier, and the other one is the optimization of the CLC reactor. The inter-connected fluidized bed reactor was proposed as the most suitable choice for chemical looping processes. During the past decade, reactors with different configurations were developed at Chalmers University of Technology (Sweden) (Berguerand and Lyngfelt, 2008a; Markström et al., 2014), *C.S.I.C.* (Spain) (Cuadrat et al., 2011), Southeast University (China) (Shen et al., 2010b, 2009b), Guangzhou Institute of Energy Conversion (China) (Wei et al., 2015), Huazhong University of Science & Technology (HUST, China) (Ma et al., 2018a, 2015b), Ohio State University (USA) (Fan, 2011), Western Kentucky University (USA) (Cao et al., 2012), IFP Energies Nouvelles (France) (Sozinho et al., 2012), and Hamburg University of Technology (Germany) (Thon et al., 2014) et al. Moreover, three MW-level industrial CLC plants have been demonstrated by Darmstadt University of Technology in Germany (Ströhle et al., 2015), Alstom Power in USA (Abdulally et al., 2011), and Chalmers University of Technology. (Berdugo Vilches et al., 2017).

The development of CLC reactor at HUST has experienced four stages since 2010, as shown in Fig. 22: 1) construction of the cold-flow model reactor and hydrodynamic investigation; 2) implementation of the 5 kW_{th} lab-scale inter-connected fluidized bed reactor; 3) demonstration of the 50 kW_{th} *i*G-CLC reactor based on the operation experience and reactor design optimization of the 5 kW_{th} reactor; 4) scale-up of the CLC reactor to MW-level *via* CFD simulation.

3.1. Cold-flow reactor model

For the investigation of a complex reactor like the CLC system, operation of a cold-flow model is essential before the construction of hot-mode reactor. Moreover, it is much easier to run the cold-flow model reactor and the running experience can provide guidance for the hot-mode reactor design. Based on the scaling rules, the geometric dimension of the cold-flow model can be calculated from the hot prototype. Due to the implacable constraint conditions, the scaling rules were simplified by choosing several key factors to meet the requirements. (Markström and Lyngfelt, 2012) With this in mind, several sets of full-scale cold-flow model reactor (a representative one is schematically shown in Fig. 23) were built to investigate the detailed fluid dynamics and oxygen carrier circulation behavior within the system. (Ma et al., 2012) With respect to the cold-flow model reactor, it mainly consists of the air reactor (AR), fuel reactor (FR), riser, loop seal (LS), down comer (DC), and cyclone (CY). The design principles of each parts are as follows:

AR: The superficial gas velocity in the AR was designed in the bubbling or turbulent fluidized regime depending on the superficial air velocity (usually, less than 1.0 U_t for air, here U_t is the terminal velocity of the oxygen carrier). The turbulent fluidized bed will possess homogeneous distribution of gas-solid phases and relatively small pressure fluctuation.

FR: It was set as a bubbling fluidized bed (typically, 15 U_{mf}, where U_{mf} is the minimum fluidization velocity of the oxygen carrier). The solid inventory was calculated to be 2000 kg/MW_{th} for the hematite oxygen carrier, which could guarantee sufficient lattice oxygen for coal conversion.

Riser: The riser was adopted to provide the driving force for oxygen carrier circulation. For the AR and FR, the oxygen carrier circulation routes here were independent. Therefore, the limitation of the overflow effect on the solid circulation can be overcome. The superficial gas velocity in the riser was set to be increased by the decreased cross-sectional area.

LS: Bidirectional loop seal (LS2) was designed for this reactor system. The first chamber was connected with the lower part of the AR to transport the reduced oxygen carrier, which formed a loop from AR, LS1, FR, LS2, and finally to the AR. The second chamber was located in the middle of LS2 and connected with the down comer (DC2) to store oxygen carrier as well as to balance the pressure difference between DC2 and the two reactors. The third chamber was linked to the FR to receive and transport part of the reduced oxygen carrier from FR. It also helped to balance the different solid circulation rates in AR and FR under different operation parameters, by forming the inner circulation of solid particles from FR, LS2, and finally to FR.

DC: A relatively large cross-sectional area was designed for the DC due to the high solid circulation rate in the reactor. The height of the DC was increased by 1.5 times of the calculated value in order to balance the pressure difference.

CY: Two series wound cyclones were designed based on the density difference of oxygen carrier and coal ash, in which the first cyclone was used for the separation of oxygen carrier and the second one was used for separation of coal ash.

A series of continuous operation tests were conducted to investigate the effects of different operational parameters, including superficial velocity, and solid inventory in both AR and FR, on the pressure drop, gas leakage, and particle attrition rate. Moreover, long-term continuous operation verified the stability and maneuverability of the reactor. The design and operation experience of the cold-flow model reactor laid basis for the design and construction of the hot prototype.

3.2. Lab-scale inter-connected fluidized bed reactor (5 kW_{th})

Based on the design and operation experience of the cold-flow model reactor, a 5 kW_{th} lab-scale inter-connected fluidized bed reactor for CLC was developed (Ma et al., 2015a). As shown in Fig. 24, a bubbling-fluidized bed combined with a fast-fluidized bed (riser) was adopted as FR to guarantee enough fuel residence time and to provide the driving force for oxygen carrier circulation, while the AR was mainly operated as a turbulent-fluidized bed. To be noted, the original hot reactor was configured with a bidirectional loop seal, but the particle circulation from the loop seal to the fuel reactor was artificially blocked due to the practical operation difficulty. Performance of the CLC reactor under different operation parameters (FR bed inventory, reaction temperature, gas superficial velocity, et al.) were evaluated, in terms of cyclone efficiency and gas leakage. For the tests with fuels

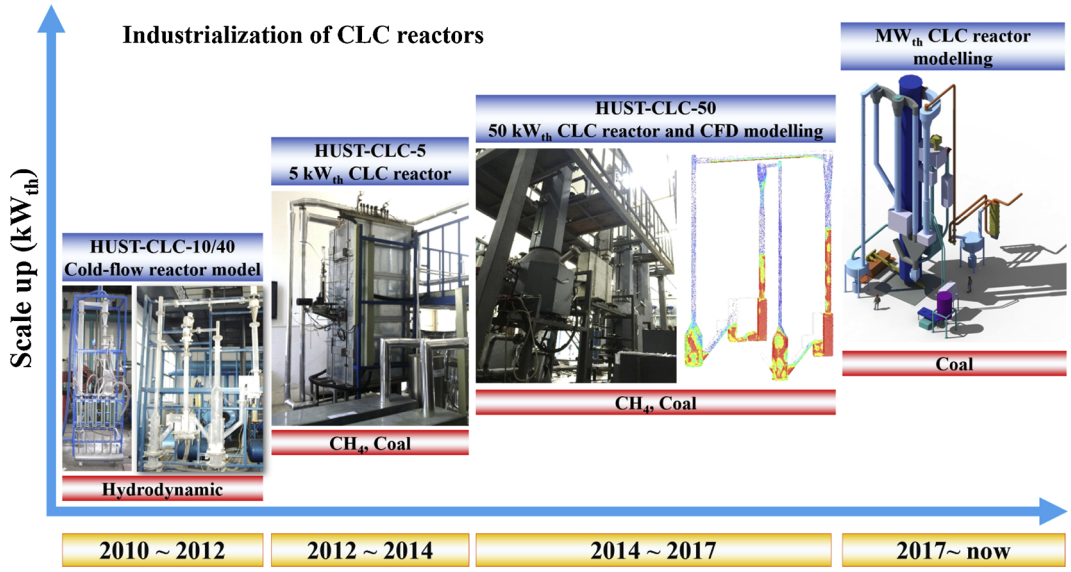

Fig. 22. Development of CLC reactors at HUST.

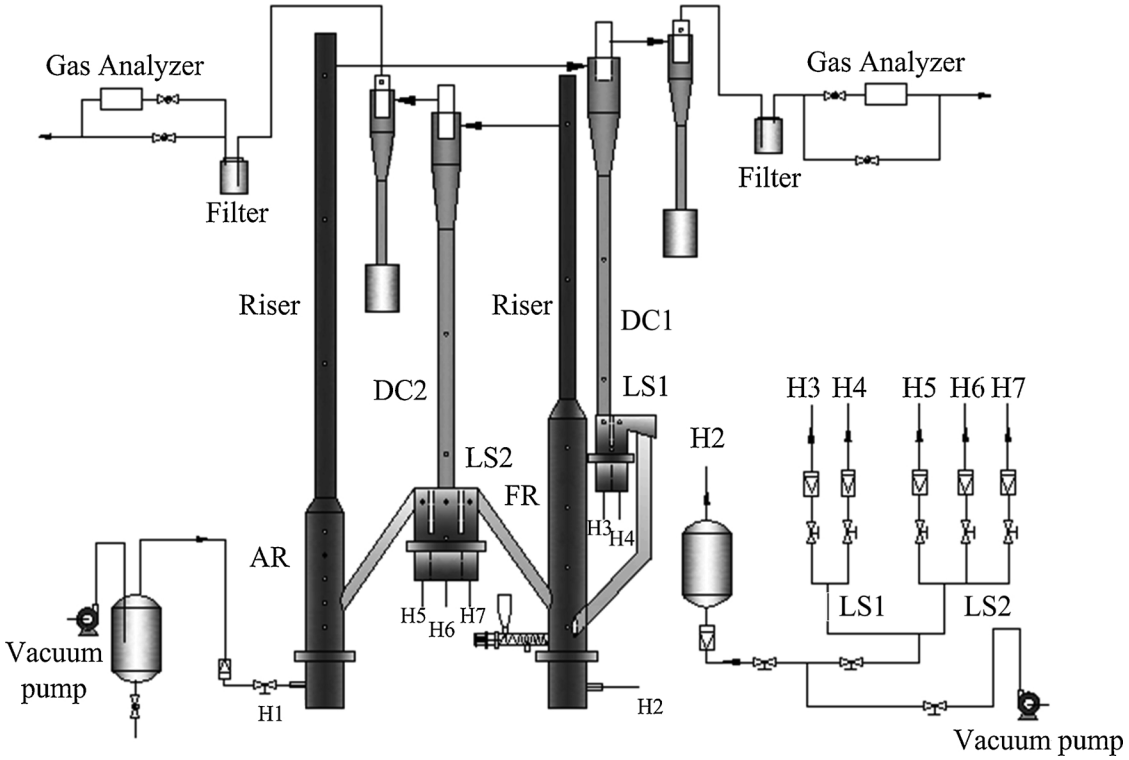

Fig. 23. Sketch map of the cold-flow model reactor. (Ma et al., 2012).

(CH_4 and coal), inexpensive natural hematite was used as oxygen carrier, and a total of 300 h of continuous running was attained.

3.2.1. Reactor performance

First of all, the cyclone separation efficiency was investigated at the initial 3.5 h continuous running. Due to the adhesion of pretty fine powders at the surface of the oxygen carrier particle (as verified by SEM results), relatively low cyclone separation efficiency was attained at the first 15 min. Nevertheless, after the elimination of fine powders from the oxygen carrier surface, high cyclone separation efficiency of 99 % could be achieved for all tests, which demonstrated the feasibility of the cyclone system of inter-connected fluidized bed reactor.

The gas leakage between AR and FR was examined by varying the gas flow rates in FR (F_{FR}). F_{FR} was maintained at 28 l/min during the first 60 min and then decreased to 20 l/min during the second stage (60 – 120 min). The average gas leakage rate in the first stage was 1.8 % and then increased to 3.2 % with the decrease of F_{FR} to 20 L/min. This result was anticipated, as with the decrease of F_{FR}, the standard deviation of pressure drop in the FR would be much larger due to the growth and break of bubbles, which eventually resulted in more significant pressure fluctuation in the FR. The pressure fluctuation would lead to unsteady pressure difference between the FR and LS, and thus affected the bed height in the down comer of FR, which contributed to more severe gas leakage between FR and AR.

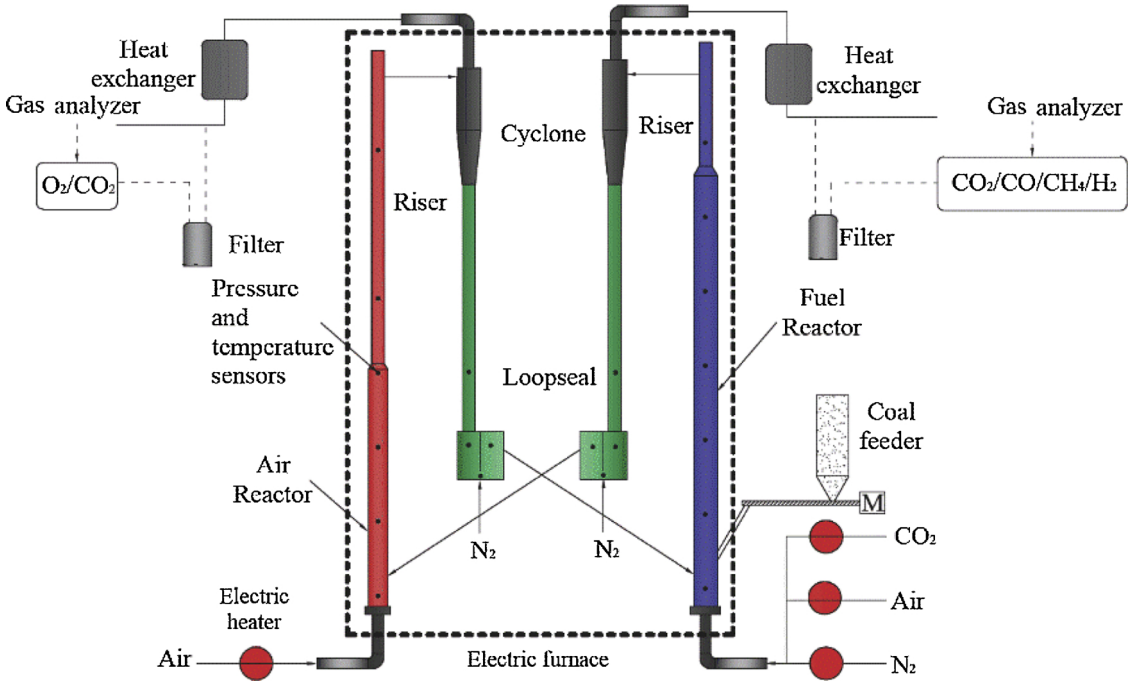

Fig. 24. A schematic view of the 5 kW_{th} CLC reactor. (Ma et al., 2015a).

3.2.2. CH_4-fueled CLC

For the test with CH_4, a total of 100 h continuous operation was achieved with hematite as oxygen carrier, at different FR temperatures (900 − 1000 °C), thermal power inputs (1.0–1.5 kW_{th}), gas flow rates in FR (20 − 28 L/min), and solid inventories (2.0–2.5 kg). (Ma et al., 2015b) The effects of different operational parameters on the performance of the CLC reactor were investigated. The results showed that the highest CH_4 conversion that could be achieved was only 81.4 % at 1000 °C, which indicated the limited reactivity of the hematite oxygen carrier towards CH_4. Carbon deposition due to CH_4 decomposition was found to be detrimental to the carbon capture efficiency. Moreover, the gas leakage from FR to AR also decreased the carbon capture efficiency. Sufficient bed inventory in the FR could benefit the CO_2 yield by providing enough lattice oxygen to combust fuel gases. It should be noted that further optimization of the operation temperature is required to balance the CH_4 conversion and CO_2 yield when using this hematite as oxygen carrier. Higher temperature could be beneficial for CH_4 conversion but would result in more severe carbon deposition.

The hematite oxygen carrier used in the continuous test showed no obvious sintering issue. TGA tests were conducted to characterize the reactivity of both the fresh and used oxygen carriers towards simulated coal-derived syngas. The results showed that the oxygen transport capacity of the used hematite oxygen carrier decreased in comparison to the fresh sample. However, the reaction rates attained with the used sample were slightly higher than that of the fresh sample in both reduction stage and air oxidization stage. This can be attributed to the activation of the hematite oxygen carrier under cyclic redox reaction scheme. (Adánez et al., 2010)

3.2.3. Coal-fueled CLC

Based on the operational experience attained in CH_4 test, solid fuel (bituminous coal) was further investigated in the continuous CLC reactor. (Ma et al., 2015a) The operation temperature of FR was found to significantly affect the combustion efficiency and CO_2 yield, which was attributed to the high temperature dependence of the oxygen carrier activity. The highest combustion efficiency was attained as 96.3 % at 1000 °C, with a high CO_2 yield of 90 %, at the thermal power input of 2 kW_{th}. Unconverted CH_4 was observed at the outlet of FR, due to the limited activity of the hematite oxygen carrier towards CH_4 (Ma et al., 2015b), while the unconverted CO was attributed to the short residence time of coal in the FR.

During the continuous running, the hematite oxygen carrier showed satisfying reactivity towards combustible gases and good sintering resistance. BET analysis of the used samples showed a slight decrease in surface area in comparison to the fresh ones. Nevertheless, tests with simulated coal-derived syngas in TGA indicated no significant activity change of the hematite oxygen carrier before and after continuous test. Overall, the low-cost and moderate reactivity of the hematite oxygen carrier made it suitable for CLC operation in large scale.

3.3. Pilot-scale inter-connected fluidized bed reactor (50 kW_{th})

In the operation of the 5 kW_{th} CLC reactor with coal, unreacted residual char in the FR was entrained into the AR by the circulation of oxygen carrier, which resulted in the decrease of CO_2 capture efficiency. To address this issue, a carbon stripper was configured after the FR to enhance the conversion of residual char in the 50 kW_{th} CLC reactor, as shown in Fig. 25. Generally, the configuration of the 50 kW_{th} CLC reactor was similar to that of the 5 kW_{th} reactor (Fig. 24), with the most different part lied in the loop seal of FR. As can be seen in Fig. 25, LS-2 was designed as a four-chamber reactor, which functioned as both a loop seal and a carbon stripper (which is different from conventional carbon stripper for physical separation of char from oxygen carrier streams). The first chamber was operated at the moving bed regime to balance the pressure difference between the two reactors, and the second and third chambers were fluidized by steam to gasify the unconverted char particles entrained by the oxygen carrier (that is, the unconverted char is chemically separated from oxygen carrier streams and the combustible gases generated therein). At the top of second and third chambers, the outlet gas (containing combustible gas species) was recycled back into the FR for further conversion, so as to improve the carbon capture efficiency. The fourth chamber was designed to transport the reduced oxygen carriers in FR to AR for oxygen capacity regeneration.

During the operation, the coal feeding rate was 7.3 kg/h, corresponding to a nominal thermal power input of 50 kW_{th}. Note that, the

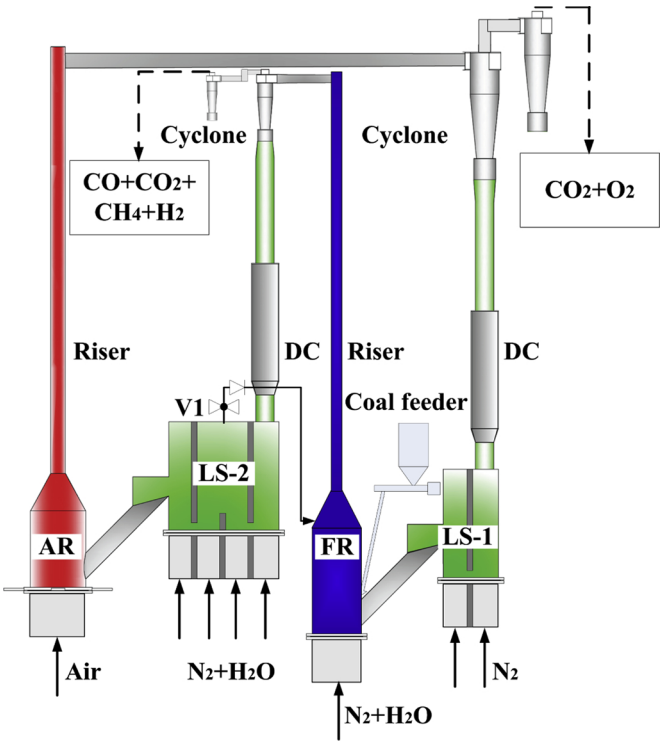

Fig. 25. Schematic view of the 50 kW_{th} *i*G-CLC reactor at HUST. (Ma et al., 2018a).

thermal power was calculated on the basis of the lower heating value of Shenhua coal (24.8 MJ/kg). A series of tests were conducted to investigate the performance of the 50 kW_{th} CLC reactor under different operational parameters. The highest CO_2 yield reached 0.91 and the combustion efficiency was 0.86, at 1000 °C during 120 min continuous running with a bed inventory of 100 kg in FR. The change of inlet gas flow rate of FR was found to exert little effect on the three CLC indices (combustion efficiency, carbon capture efficiency, and CO_2 yield). This was explained by the large amount of gas species evolved from coal conversion (mainly CO_2, H_2O), which also acted as fluidizing agents and made the change of the actual superficial gas velocity in FR insignificant when varied the inlet gas flow rates of the 50kW_{th} reactor.

3.4. Simulation and modelling of the inter-connected fluidized bed reactors

CFD simulation of the 5 kW_{th} and 50 kW_{th} CLC reactors were first conducted to support the reactor design and operation optimization. To be consistent with the tests of the 5 kW_{th} reactor, the simulations were performed in two aspects: CH_4-CLC simulation (Su et al., 2015a) and coal-CLC simulation (Su et al., 2015b). Generally, the simulation results agreed well with the experimental results to some extent, and computational particle fluid dynamics (CPFD) simulation can provide guidance for the reactor operation. For example, the simulation results can be used to predict and analyze gas leakage between AR and FR, to improve the fuel combustion efficiency by rationally decreasing the fluidization gas velocity, increasing the reactor temperature and decreasing the coal feeding rate. With respect to the 50 kW_{th} chemical looping combustor, CFD simulation (Chen et al., 2019) revealed that the combustible gases (CH_4 and CO) cannot effectively diffuse throughout the FR with only one coal feeding point, which was unfavorable for the good mixing between oxygen carriers and combustible gases. However, with two oppositely-collocated coal feeding points, well mixed gas-solid contact was achieved, which promoted the reaction between oxygen carriers and the fuel gases. Eventually, much higher CO_2 yield and combustion efficiency was attained. Meanwhile, it was found that an insufficient residence time of particles (both char and oxygen carrier) in FR is responsible for a relative low combustion efficiency. Correspondingly, a higher FR was proposed as an optimization to extend reaction path of both homogeneous and heterogeneous reactions therein.

In order to meet the requirement of fast simulation of the CLC reactor, a macroscopic model considering the flow, heat transfer and chemical reaction in the reactor was also established and then implemented in Aspen Customer Modeler (ACM) platform, and finally applied to the modeling of the FR (including the riser). The results showed that the reaction temperature was the most important factor to affect the combustion efficiency and CO_2 capture efficiency, and the two indices both increased with the reaction temperature. The increase of oxygen to fuel ratio would also increase the combustion efficiency but decrease the CO_2 capture efficiency, while increasing the CO_2 proportion in fluidization gas showed the opposite effect. (Xu et al., 2018) The macroscopic model and fast simulation will be further developed for the simulation of full-scale CLC reactors (including AR, FR, and possibly loop seal and carbon stripper) and their scaling-up.

4. Summary and outlook

The unique advantages in utilizing lattice oxygen of oxygen carrier instead of gaseous O_2 in air make the chemical looping technique very attractive for fuel combustion, conversion, or value-added chemicals production. During the past decades, continued research in chemical looping processes has resulted in the development of novel oxygen carriers, new research methods, and pilot-scale chemical looping reactors.

Over 100 different kinds of oxygen carriers developed at Huazhong University of Science & Technology (HUST) have been comprehensively reviewed in terms of redox reactivity, cyclic stability, and economical efficiency under different chemical looping schemes (CLC, *i*G-CLC, CLOU, CLAS, CLG, *etc.*) in this article. Among all the reviewed oxygen carriers, the CuO@TiO_2-Al_2O_3 oxygen carrier is distinguished for its high reaction performance as well as superior sintering resistance in CLOU and CLAS processes; while the cement bonded fine hematite and copper ore oxygen carrier is promising for *i*G-CLC of coal, owing to its synergistic reactivity, high physicochemical stability and low cost. Novel application of the chemical looping concept to dechlorination in plastic waste treatment was demonstrated with CaO-decorated Fe_2O_3/Al_2O_3 oxygen carrier. The PCDD/Fs inhibition mechanism within the *i*G-CLC context was found to be attributed to the suppress of precursor conversion and *de novo* synthesis of PCDD/Fs as well as the limitation of Deacon reaction in O_2-free environment.

The development of CLC reactors were conducted in parallel with the investigation on oxygen carriers. From cold flow reactor model, lab-scale inter-connected fluidized bed reactor (5 kW_{th}) and pilot-scale CLC reactor (50 kW_{th}) to MW-level reactor design and simulation, extensive experience on reactor running and reactor design optimization have been attained. Over 300 h of combined running of the 5 kW_{th} and 50 kW_{th} CLC reactors was achieved, using inexpensive iron ore as oxygen carrier, and both CH_4 and coal as fuels.

In addition to experimental investigations, modelling and simulation at various scales are also highlighted to gain insight into details and underlying mechanism. DFT calculations, MD simulation, and CFD simulations were also conducted for assistance in the investigation: DFT calculation results gave in-depth understanding of the reaction and interaction mechanism of the oxygen carrier/inert support system, which were beneficial for rational synthesis of high-performance oxygen carriers and exploring reaction mechanism and kinetics involved in chemical looping processes; MD simulation was recently conducted to understand the sintering of CuO nanograin; CFD simulation results provided guidance for the running of the inter-connected fluidized bed reactor, which eventually helped the optimization of both the reactor design and operational parameters in an economical way

rather than by means of costly and tedious experiment.

With the continuing and rapid development of chemical looping technologies, the traditional trail-and-error method for oxygen carrier screening is not adequate from both efficiency and economy standpoints. Thus, new insights in tailoring the reaction and physiochemical properties of oxygen carriers are highly desirable to realize rational design of oxygen carriers. Meanwhile, it is highly required to realize large-scale preparation of OC particles and achieve optimal matching among oxygen carrier, fuel, and reactor in terms of cost and efficiency. Moreover, due to the different reaction atmosphere in chemical looping processes in comparison to traditional fuel conversion processes, detailed reaction kinetics involved in chemical looping processes should be carefully determined so as to achieve more accurate and reliable kinetics data for CFD simulation. Additionally, growing interests are being shown on new applications of the chemical looping scheme, like the chemical looping oxidative cracking of naphtha that we have tried recently for light olefins production. As can be expected, the development of chemical looping-related techniques will witness an extensive expand in the following years and implementation of industrial scale units is highly promising in the medium-term.

Declaration of Competing Interest

The authors declare that they have no known competing financial interests or personal relationships that could have appeared to influence the work reported in this paper.

Acknowledgements

These authors were supported by “National Key R&D Program of China (2016YFB0600801)” and “National Natural Science Foundation of China (51522603)”.

References

Abad, A., Adánez-Rubio, I., Gayán, P., García-Labiano, F., Luis, F., Adánez, J., 2012a. Demonstration of chemical-looping with oxygen uncoupling (CLOU) process in a 1.5 kW_{th} continuously operating unit using a Cu-based oxygen-carrier. Int. J. Greenh. Gas Con. 6, 189–200.

Abad, A., Adánez, J., Cuadrat, A., García-Labiano, F., Gayán, P., Luis, F., 2011. Kinetics of redox reactions of ilmenite for chemical-looping combustion. Chem. Eng. Sci. 66, 689–702.

Abad, A., Adánez, J., Gayán, P., Luis, F., García-Labiano, F., Sprachmann, G., 2015a. Conceptual design of a 100 MW_{th} CLC unit for solid fuel combustion. Appl. Energy 157, 462–474.

Abad, A., Cuadrat, A., Mendiara, T., García-Labiano, F., Gayán, P., de Diego, L., Adánez, J., 2012b. Low-Cost Fe-Based oxygen carrier materials for the iG-CLC process with coal. 2. Ind. Eng. Chem. Res. 51, 16230–16241.

Abad, A., García-Labiano, F., de Diego, L.F., Gayán, P., Adánez, J., 2007a. Reduction kinetics of Cu-, Ni-, and Fe-based oxygen carriers using syngas ($CO + H_2$) for chemical-looping combustion. Energy Fuel 21, 1843–1853.

Abad, A., Mattisson, T., Lyngfelt, A., Johansson, M., 2007b. The use of iron oxide as oxygen carrier in a chemical-looping reactor. Fuel 86, 1021–1035.

Abad, A., Mattisson, T., Lyngfelt, A., Rydén, M., 2006. Chemical-looping combustion in a 300 W continuously operating reactor system using a manganese-based oxygen carrier. Fuel 85, 1174–1185.

Abad, A., Mendiara, T., de Diego, L., García-Labiano, F., Gayán, P., Adánez, J., 2018. A simple model for comparative evaluation of different oxygen carriers and solid fuels in iG-CLC processes. Fuel Process. Technol. 179, 444–454.

Abad, A., Pérez-Vega, R., Luis, F., García-Labiano, F., Gayán, P., Adánez, J., 2015b. Design and operation of a 50 kW_{th} Chemical Looping Combustion (CLC) unit for solid fuels. Appl. Energy 157, 295–303.

Abdulally, I., Edberg, C., Andrus, H., Chiu, J., Thibeault, P., Lani, P., 2011. ALSTOM's Chemical Looping Combustion Prototype for CO_2 Capture From Existing Pulverized Coal-fired Power Plants. NETL Project NT0005286.

Adánez-Rubio, I., Abad, A., Gayán, P., García-Labiano, F., Luis, F., Adánez, J., 2014. The fate of sulphur in the Cu-based Chemical Looping with oxygen uncoupling (CLOU) process. Appl. Energy 113, 1855–1862.

Adanez, J., Abad, A., Garcia-Labiano, F., Gayan, P., Luis, F., 2012. Progress in chemical-looping combustion and reforming technologies. Prog. Energy Combust. Sci. 38, 215–282.

Adánez, J., Abad, A., Mendiara, T., Gayán, P., de Diego, L.F., García-Labiano, F., 2018. Chemical looping combustion of solid fuels. Prog. Energy Combust. Sci. 65, 6–66.

Adánez, J., Cuadrat, A., Abad, A., Gayán, P., de Diego, L.F., García-Labiano, F., 2010. Ilmenite activation during consecutive redox cycles in chemical-looping combustion. Energy Fuel 24, 1402–1413.

Adánez, J., Gayán, P., Celaya, J., de Diego, L.F., García-Labiano, F., Abad, A., 2006. Chemical looping combustion in a 10 kW_{th} prototype using a CuO/Al_2O_3 oxygen carrier: effect of operating conditions on methane combustion. Ind. Eng. Chem. Res. 45, 6075–6080.

Adánez, Jd., de Diego, L.F., García-Labiano, F., Gayán, P., Abad, A., Palacios, J., 2004. Selection of oxygen carriers for chemical-looping combustion. Energy Fuel 18, 371–377.

Arjmand, M., Azad, A.-M., Leion, H., Mattisson, T., Lyngfelt, A., 2012. Evaluation of $CuAl_2O_4$ as an oxygen carrier in chemical-looping combustion. Ind. Eng. Chem. Res. 51, 13924–13934.

Bao, J., Li, Z., Cai, N., 2013a. Promoting the reduction reactivity of ilmenite by introducing foreign ions in chemical looping combustion. Ind. Eng. Chem. Res. 52, 6119–6128.

Bao, J., Li, Z., Cai, N., 2013b. Reduction kinetics of foreign-ion-promoted ilmenite using carbon monoxide (CO) for chemical looping combustion. Ind. Eng. Chem. Res. 52, 10646–10655.

Bao, J., Li, Z., Cai, N., 2014a. Experiments of char particle segregation effect on the gas conversion behavior in the fuel reactor for chemical looping combustion. Appl. Energy 113, 1874–1882.

Bao, J., Li, Z., Cai, N., 2014b. Interaction between iron-based oxygen carrier and four coal ashes during chemical looping combustion. Appl. Energy 115, 549–558.

Bao, J., Li, Z., Sun, H., Cai, N., 2013c. Experiment and rate equation modeling of Fe oxidation kinetics in chemical looping combustion. Combust. Flame 160, 808–817.

Bayham, S.C., Kim, H.R., Wang, D., Tong, A., Zeng, L., McGiveron, O., Kathe, M.V., Chung, E., Wang, W., Wang, A., 2013. Iron-based coal direct chemical looping combustion process: 200 h continuous operation of a 25 kW_{th} subpilot unit. Energy Fuel 27, 1347–1356.

Berdugo Vilches, T., Lind, F., Rydén, M., Thunman, H., 2017. Experience of more than 1000 h of operation with oxygen carriers and solid biomass at large scale. Appl. Energy 190, 1174–1183.

Berguerand, N., Lyngfelt, A., 2008a. Design and operation of a 10 kW_{th} chemical-looping combustor for solid fuels – testing with South African coal. Fuel 87, 2713–2726.

Berguerand, N., Lyngfelt, A., 2008b. The use of petroleum coke as fuel in a 10 kW_{th} chemical-looping combustor. Int. J. Greenh. Gas Con. 2, 169–179.

Brunet, S., Mey, D., Pérot, G., Bouchy, C., Diehl, F., 2005. On the hydrodesulfurization of FCC gasoline: a review. Appl. Catal. A-Gen 278, 143–172.

Cao, Y., Sit, S.P., Pan, W.P., 2012. The development of 10 kW chemical looping combustion technology in ICSET, WKU. 2nd International Conference on Chemical Looping 26–28.

Chen, X., Ma, J., Tian, X., Wan, J., Zhao, H., 2019. CPFD simulation and optimiaztion of a 50 kWth dual circulating fluizied bed reactor for chemcial looping combsution of coal. Int. J. Greenh. Gas Con. 90, 102800.

Chuang, S., Dennis, J., Hayhurst, A., Scott, S., 2008. Development and performance of Cu-based oxygen carriers for chemical-looping combustion. Combust. Flame 154, 109–121.

Chuang, S., Dennis, J., Hayhurst, A., Scott, S., 2009. Kinetics of the chemical looping oxidation of CO by a co-precipitated mixture of CuO and Al_2O_3. Proc. Combust. Inst. 32, 2633–2640.

Clayton, C.K., Whitty, K.J., 2014. Measurement and modeling of decomposition kinetics for copper oxide-based chemical looping with oxygen uncoupling. Appl. Energy 116, 416–423.

Cuadrat, A., Abad, A., García-Labiano, F., Gayán, P., de Diego, L.F., Adánez, J., 2011. The use of ilmenite as oxygen-carrier in a 500 W_{th} Chemical-Looping Coal Combustion unit. Int. J. Greenh. Gas Con. 5, 1630–1642.

de Diego, L.F., García-Labiano, F., Gayán, P., Abad, A., Cabello, A., Adánez, J., Sprachmann, G., 2014. Performance of Cu- and Fe-based oxygen carriers in a 500 W_{th} CLC unit for sour gas combustion with high H_2S content. Int. J. Greenh. Gas Con. 28, 168–179.

Dudek, R.B., Tian, X., Blivin, M., Neal, L.M., Zhao, H., Li, F., 2019. Perovskite oxides for redox oxidative cracking of *n*-Hexane under a cyclic redox scheme. Appl. Catal. B-Environ. 246, 30–40.

Fan, L., 2011. Chemical Looping Systems for Fossil Energy Conversions. John Wiley Sons.

Galinsky, N., Mishra, A., Zhang, J., Li, F., 2015. $Ca_{1-x}A_xMnO_3$ (A = Sr and Ba) perovskite based oxygen carriers for chemical looping with oxygen uncoupling (CLOU). Appl. Energy 157, 358–367.

Galinsky, N., Sendi, M., Bowers, L., Li, F., 2016. $CaMn_{1-x}B_xO_{3-\delta}$ (B = Al, V, Fe, Co, and Ni) perovskite based oxygen carriers for chemical looping with oxygen uncoupling (CLOU). Appl. Energy 174, 80–87.

García-Labiano, F., de Diego, L.F., Adánez, J., Abad, A., Gayán, P., 2004. Reduction and oxidation kinetics of a copper-based oxygen carrier prepared by impregnation for chemical-looping combustion. Ind. Eng. Chem. Res. 43, 8168–8177.

García-Labiano, F., Luis, F., Adánez, J., Abad, A., Gayán, P., 2005. Temperature variations in the oxygen carrier particles during their reduction and oxidation in a chemical-looping combustion system. Chem. Eng. Sci. 60, 851–862.

Gayán, P., Adánez-Rubio, I., Abad, A., de Diego, L.F., García-Labiano, F., Adánez, J., 2012. Development of Cu-based oxygen carriers for chemical-looping with Oxygen Uncoupling (CLOU) process. Fuel 96, 226–238.

Gayán, P., Luis, F., García-Labiano, F., Adánez, J., Abad, A., Dueso, C., 2008. Effect of support on reactivity and selectivity of Ni-based oxygen carriers for chemical-looping combustion. Fuel 87, 2641–2650.

Ge, H., Guo, W., Shen, L., Song, T., Xiao, J., 2016. Biomass gasification using chemical looping in a 25 kW_{th} reactor with natural hematite as oxygen carrier. Chem. Eng. J. 286, 174–183.

Ge, H., Shen, L., Gu, H., Jiang, S., 2015. Effect of co-precipitation and impregnation on K-decorated Fe_2O_3/Al_2O_3 oxygen carrier in Chemical Looping Combustion of

bituminous coal. Chem. Eng. J. 262, 1065–1076.
Goldstein, E.A., Mitchell, R.E., 2011. Chemical kinetics of copper oxide reduction with carbon monoxide. Proc. Combust. Inst. 33, 2803–2810.
Gu, H., Shen, L., Xiao, J., Zhang, S., Song, T., Chen, D., 2012. Iron ore as oxygen carrier improved with potassium for chemical looping combustion of anthracite coal. Combust. Flame 159, 2480–2490.
Gu, H., Shen, L., Zhong, Z., Niu, X., Liu, W., Ge, H., Jiang, S., Wang, L., 2015. Cement/CaO-modified iron ore as oxygen carrier for chemical looping combustion of coal. Appl. Energy 157, 314–322.
Guo, L., Zhao, H., Wang, K., Mei, D., Ma, Z., Zheng, C., 2016. Reduction kinetics analysis of sol–gel-derived $CuO/CuAl_2O_4$ oxygen carrier for chemical looping with oxygen uncoupling. J. Therm. Anal. Calorim. 123, 745–756.
Guo, L., Zhao, H., Zheng, C., 2015. Synthesis gas generation by chemical-looping reforming of biomass with natural copper ore as oxygen carrier. Waste Biomass Valori. 6, 81–89.
Guo, L., Zhao, H., Ma, J., Mei, D., Zheng, C., 2014. Comparison of Large-scale production methods of Fe_2O_3/Al_2O_3 oxygen carriers for chemical-looping combustion. Chem. Eng. Tchnol. 37, 1211–1219.
Håkonsen, S.F., Blom, R., 2011. Chemical looping combustion in a rotating bed reactor–finding optimal process conditions for prototype reactor. Environ. Sci. Technol. 45, 9619–9626.
Håkonsen, S.F., Grande, C.A., Blom, R., 2014. Rotating bed reactor for CLC: bed characteristics dependencies on internal gas mixing. Appl. Energy 113, 1952–1957.
He, F., Li, F., 2015. Perovskite promoted iron oxide for hybrid water-splitting and syngas generation with exceptional conversion. Energy Environ. Sci. 8, 535–539.
He, F., Li, X., Zhao, K., Huang, Z., Wei, G., Li, H., 2013. The use of $La_{1-x}Sr_xFeO_3$ perovskite-type oxides as oxygen carriers in chemical-looping reforming of methane. Fuel 108, 465–473.
He, F., Trainham, J., Parsons, G., Newman, J.S., Li, F., 2014. A hybrid solar-redox scheme for liquid fuel and hydrogen coproduction. Energy Environ. Sci. 7, 2033–2042.
Hossain, M.M., de Lasa, H.I., 2008. Chemical-looping combustion (CLC) for inherent CO_2 separations—a review. Chem. Eng. Sci. 63, 4433–4451.
Hossain, M.M., de Lasa, H.I., 2010. Reduction and oxidation kinetics of $Co–Ni/Al_2O_3$ oxygen carrier involved in a chemical-looping combustion cycles. Chem. Eng. Sci. 65, 98–106.
Imtiaz, Q., Broda, M., Müller, C.R., 2014. Structure–property relationship of co-precipitated Cu-rich, Al_2O_3-or $MgAl_2O_4$-stabilized oxygen carriers for chemical looping with oxygen uncoupling (CLOU). Appl. Energy 119, 557–565.
Imtiaz, Q., Hosseini, D., Müller, C.R., 2013. Review of oxygen carriers for chemical looping with oxygen uncoupling (CLOU): thermodynamics, material development, and synthesis. Energy Technol. 1, 633–647.
Ishida, M., Jin, H., 1994. A new advanced power-generation system using chemical-looping combustion. Energy 19, 415–422.
Ishida, M., Jin, H., 1996. A novel chemical-looping combustor without NO_x formation. Ind. Eng. Chem. Res. 35, 2469–2472.
Ishida, M., Jin, H., Okamoto, T., 1996. A fundamental study of a new kind of medium material for chemical-looping combustion. Energy Fuel 10, 958–963.
Jerndal, E., Leion, H., Axelsson, L., Ekvall, T., Hedberg, M., Johansson, K., Källen, M., Svensson, R., Mattisson, T., Lyngfelt, A., 2011. Using low-cost iron-based materials as oxygen carriers for chemical looping combustion. Oil Gas Sci. Technol. 66, 235–248.
Jin, H., Ishida, M., 2002. Reactivity study on natural-gas-fueled chemical-looping combustion by a fixed-bed reactor. Ind. Eng. Chem. Res. 41, 4004–4007.
Johansson, M., Mattisson, T., Lyngfelt, A., 2004. Investigation of Fe_2O_3 with $MgAl_2O_4$ for chemical-looping combustion. Ind. Eng. Chem. Res. 43, 6978–6987.
Leion, H., Jerndal, E., Steenari, B.-M., Hermansson, S., Israelsson, M., Jansson, E., Johnsson, M., Thunberg, R., Vadenbo, A., Mattisson, T., 2009a. Solid fuels in chemical-looping combustion using oxide scale and unprocessed iron ore as oxygen carriers. Fuel 88, 1945–1954.
Leion, H., Larring, Y., Bakken, E., Bredesen, R., Mattisson, T., Lyngfelt, A., 2009b. Use of $CaMn_{0.875}Ti_{0.125}O_3$ as oxygen carrier in chemical-looping with oxygen uncoupling. Energy Fuel 23, 5276–5283.
Leion, H., Mattisson, T., Lyngfelt, A., 2007. The use of petroleum coke as fuel in chemical-looping combustion. Fuel 86, 1947–1958.
Li, F., Sun, Z., Luo, S., Fan, L., 2011. Ionic diffusion in the oxidation of iron—effect of support and its implications to chemical looping applications. Energy Environ. Sci. 4, 876–880.
Li, Z., Zhang, T., Cai, N., 2008. Experimental study of O_2-CO_2 production for the oxyfuel combustion using a Co-based oxygen carrier. Ind. Eng. Chem. Res. 47, 7147–7153.
Lind, F., Seemann, M., Thunman, H., 2011. Continuous catalytic tar reforming of biomass derived raw gas with simultaneous catalyst regeneration. Ind. Eng. Chem. Res. 50, 11553–11562.
Linderholm, C., Abad, A., Mattisson, T., Lyngfelt, A., 2008. 160 h of chemical-looping combustion in a 10 kW reactor system with a NiO-based oxygen carrier. Int. J. Greenh. Gas Con. 2, 520–530.
Linderholm, C., Schmitz, M., 2016. Chemical-looping combustion of solid fuels in a 100 kW dual circulating fluidized bed system using iron ore as oxygen carrier. J. Environ. Chem. Eng. 4, 1029–1039.
Lu, C., Li, K., Wang, H., Zhu, X., Wei, Y., Zheng, M., Zeng, C., 2018. Chemical looping reforming of methane using magnetite as oxygen carrier: structure evolution and reduction kinetics. Appl. Energy 211, 1–14.
Luis, F., Garcı, F., Gayán, P., Celaya, J., Palacios, J.M., Adánez, J., 2007. Operation of a 10 kW_{th} chemical-looping combustor during 200 h with a $CuO–Al_2O_3$ oxygen carrier. Fuel 86, 1036–1045.
Lyngfelt, A., 2014. Chemical-looping combustion of solid fuels–status of development. Appl. Energy 113, 1869–1873.
Lyngfelt, A., Leckner, B., Mattisson, T., 2001. A fluidized-bed combustion process with inherent CO_2 separation; application of chemical-looping combustion. Chem. Eng. Sci. 56, 3101–3113.
Ma, J., Mei, D., Peng, W., Tian, X., Ren, D., Zhao, H., 2019a. On the high performance of a core-shell structured $CaO-CuO/MgO@Al_2O_3$ material in calcium looping integrated with chemical looping combustion (CaL-CLC). Chem. Eng. J. 368, 504–512.
Ma, J., Mei, D., Tian, X., Zhang, S., Yang, J., Wang, C., Chen, G., Zhao, Y., Zheng, C., Zhao, H., 2019b. Fate of mercury in volatiles and char during in-situ gasification chemical looping combustion of coal. Environ. Sci. Technol. 53, 7887–7892.
Ma, J., Tian, X., Wang, C., Chen, X., Zhao, H., 2018a. Performance of a 50 kW_{th} coal-fuelled chemical looping combustor. Int. J. Greenh. Gas Con. 75, 98–106.
Ma, J., Tian, X., Zhao, H., Bhattacharya, S., Rajendran, S., Zheng, C., 2017a. Investigation of two hematites as oxygen carrier and two low-rank coals as fuel in chemical looping combustion. Energy Fuel 31, 1896–1903.
Ma, J., Wang, C., Zhao, H., Tian, X., 2018b. Sulfur fate during lignite pyrolysis process in chemical looping combustion environment. Energy Fuel 32, 4493–4501.
Ma, J., Wang, J., Tian, X., Zhao, H., 2019c. In-situ gasification chemical looping combustion of plastic waste in a semi-continuously operated fluidized bed reactor. Proc. Combust. Inst. 37, 4389–4397.
Ma, J., Zhao, H., Mei, D., Guo, L., Zheng, C., 2012. Cold-flow model experiment of interconnected fluidized bed for chemical looping combustion of coal. J. Chin. Soc. Power Eng. 32, 909–915 in Chinese.
Ma, J., Zhao, H., Tian, X., Wei, Y., Rajendran, S., Zhang, Y., Bhattacharya, S., Zheng, C., 2015a. Chemical looping combustion of coal in a 5 kW_{th} interconnected fluidized bed reactor using hematite as oxygen carrier. Appl. Energy 157, 304–313.
Ma, J., Zhao, H., Tian, X., Wei, Y., Zhang, Y., Zheng, C., 2015b. Continuous operation of interconnected fluidized bed reactor for chemical looping combustion of CH_4 using hematite as oxygen carrier. Energy Fuel 29, 3257–3267.
Ma, S., Li, M., Wang, G., Zhang, L., Chen, S., Sun, Z., Hu, J., Zhu, M., Xiang, W., 2018c. Effects of Zr doping on Fe_2O_3/CeO_2 oxygen carrier in chemical looping hydrogen generation. Chem. Eng. J. 346, 712–725.
Markström, P., Linderholm, C., Lyngfelt, A., 2014. Operation of a 100 kW chemical-looping combustor with Mexican petroleum coke and Cerrejón coal. Appl. Energy 113, 1830–1835.
Markström, P., Lyngfelt, A., 2012. Designing and operating a cold-flow model of a 100 kW chemical-looping combustor. Powder Technol. 222, 182–192.
Mattisson, T., 2013. Materials for chemical-looping with oxygen uncoupling. ISRN Chem. Eng.
Mattisson, T., Johansson, M., Lyngfelt, A., 2006. The use of NiO as an oxygen carrier in chemical-looping combustion. Fuel 85, 736–747.
Mattisson, T., Leion, H., Lyngfelt, A., 2009a. Chemical-looping with oxygen uncoupling using CuO/ZrO_2 with petroleum coke. Fuel 88, 683–690.
Mattisson, T., Lyngfelt, A., Leion, H., 2009b. Chemical-looping with oxygen uncoupling for combustion of solid fuels. Int. J. Greenh. Gas Con. 3, 11–19.
Matzen, M., Pinkerton, J., Wang, X., Demirel, Y., 2017. Use of natural ores as oxygen carriers in chemical looping combustion: a review. Int. J. Greenh. Gas Con. 65, 1–14.
Mei, D., Zhao, H., Yang, W., Fang, Y., Zheng, C., 2013a. Oxygen release kinetics and mechanism study on Cu-, Co-, Mn-based oxygen carrier. J. Fuel Chem. Technol. 41, 235–242.
Mei, D., Abad, A., Zhao, H., Adánez, J., 2015a. Characterization of a sol–gel derived $CuO/CuAl_2O_4$ oxygen carrier for chemical looping combustion (CLC) of gaseous fuels: relevance of gas–solid and oxygen uncoupling reactions. Fuel Process. Technol. 133, 210–219.
Mei, D., Abad, A., Zhao, H., Adánez, J., Zheng, C., 2014. On a highly reactive Fe_2O_3/Al_2O_3 oxygen carrier for in situ gasification chemical looping combustion. Energy Fuel 28, 7043–7052.
Mei, D., Mendiara, T., Abad, A., De Diego, L., García-Labiano, F., Gayán, P., Adánez, J., Zhao, H., 2015b. Evaluation of manganese minerals for chemical looping combustion. Energy Fuel 29, 6605–6615.
Mei, D., Mendiara, T., Abad, A., de Diego, L.F., García-Labiano, F., Gayán, P., Adánez, J., Zhao, H., 2016. Manganese minerals as oxygen carriers for chemical looping combustion of coal. Ind. Eng. Chem. Res. 55, 6539–6546.
Mei, D., Zhao, H., Ma, Z., Zheng, C., 2013b. Using the sol–gel-derived $CuO/CuAl_2O_4$ oxygen carrier in chemical looping with oxygen uncoupling for three typical coals. Energy Fuel 27, 2723–2731.
Mei, D., Zhao, H., Yan, S., 2018. Kinetics model for the reduction of Fe_2O_3/Al_2O_3 by CO in chemical looping combustion. Chem. Eng. Process. 124, 137–146.
Mendiara, T., Abad, A., De Diego, L., García-Labiano, F., Gayán, P., Adánez, J., 2013. Biomass combustion in a CLC system using an iron ore as an oxygen carrier. Int. J. Greenh. Gas Con. 19, 322–330.
Mendiara, T., Pérez, R., Abad, A., De Diego, L., García-Labiano, F., Gayán, P., Adánez, J., 2012. Low-cost Fe-based oxygen carrier materials for the iG-CLC process with coal. 1. Ind. Eng. Chem. Res. 51, 16216–16229.
Michalsky, R., Avram, A., Peterson, B., Pfromm, P.H., Peterson, A., 2015. Chemical looping of metal nitride catalysts: low-pressure ammonia synthesis for energy storage. Chem. Sci. 6, 3965–3974.
Moghtaderi, B., 2009. Application of chemical looping concept for air separation at high temperatures. Energy Fuel 24, 190–198.
Neal, L.M., Shafiefarhood, A., Li, F., 2014. Dynamic methane partial oxidation using a $Fe_2O_3@$ $La_{0.8}Sr_{0.2}FeO_{3-\delta}$ core–shell redox catalyst in the absence of gaseous oxygen. ACS Catal. 4, 3560–3569.
Neal, L.M., Yusuf, S., Sofranko, J.A., Li, F., 2016. Oxidative dehydrogenation of ethane: a chemical looping approach. Energy Technol. 4, 1200–1208.
Niu, P., Ma, Y., Tian, X., Ma, J., Zhao, H., 2018. Chemical looping gasification of biomass: part I. Screening Cu-Fe metal oxides as oxygen carrier and optimizing experimental conditions. Biomass Bioenergy 108, 146–156.
Ortiz, M., de Diego, L.F., Abad, A., García-Labiano, F., Gayán, P., Adánez, J., 2012.

Catalytic activity of Ni-based oxygen-carriers for steam methane reforming in chemical-looping processes. Energy Fuel 26, 791–800.
Peng, W., Xu, Z., Luo, C., Zhao, H., 2015. Tailor-made core–Shell CaO/TiO_2–Al_2O_3 architecture as a high-capacity and long-life CO_2 sorbent. Environ. Sci. Technol. 49, 8237–8245.
Peng, W., Xu, Z., Zhao, H., 2016. Batch fluidized bed test of SATS-derived CaO/TiO_2–Al_2O_3 sorbent for calcium looping. Fuel 170, 226–234.
Pérez-Vega, R., Abad, A., Gayán, P., de Diego, L., García-Labiano, F., Adánez, J., 2017. Development of $(Mn_{0.77}Fe_{0.23})_2O_3$ particles as an oxygen carrier for coal combustion with CO_2 capture via in-situ gasification chemical looping combustion (iG-CLC) aided by oxygen uncoupling (CLOU). Fuel Process. Technol. 164, 69–79.
Qin, C., Yin, J., Feng, B., Ran, J., Zhang, L., Manovic, V., 2016. Modelling of the calcination behaviour of a uniformly-distributed CuO/$CaCO_3$ particle in Ca–Cu chemical looping. Appl. Energy 164, 400–410.
Sarshar, Z., Kleitz, F., Kaliaguine, S., 2011. Novel oxygen carriers for chemical looping combustion: $La_{1-x}Ce_xBO_3$ (B= Co, Mn) perovskites synthesized by reactive grinding and nanocasting. Energy Environ. Sci. 4, 4258–4269.
Shah, K., Moghtaderi, B., Wall, T., 2012. Selection of suitable oxygen carriers for chemical looping air separation: a thermodynamic approach. Energ. Fuel 26, 2038–2045.
Shen, L., Gao, Z., Wu, J., Xiao, J., 2010a. Sulfur behavior in chemical looping combustion with NiO/Al_2O_3 oxygen carrier. Combust. Flame 157, 853–863.
Shen, L., Wu, J., Gao, Z., Xiao, J., 2009a. Reactivity deterioration of NiO/Al_2O_3 oxygen carrier for chemical looping combustion of coal in a 10 kW_{th} reactor. Combust. Flame 156, 1377–1385.
Shen, L., Wu, J., Gao, Z., Xiao, J., 2010b. Characterization of chemical looping combustion of coal in a 1 kW_{th} reactor with a nickel-based oxygen carrier. Combust. Flame 157, 934–942.
Shen, L., Wu, J., Xiao, J., Song, Q., Xiao, R., 2009b. Chemical-looping combustion of biomass in a 10 kW_{th} reactor with iron oxide as an oxygen carrier. Energy Fuel 23, 2498–2505.
Shen, L., Zheng, M., Xiao, J., Xiao, R., 2008. A mechanistic investigation of a calcium-based oxygen carrier for chemical looping combustion. Combust. Flame 154, 489–506.
Shulman, A., Cleverstam, E., Mattisson, T., Lyngfelt, A., 2009. Manganese/iron, manganese/nickel, and manganese/silicon oxides used in chemical-looping with oxygen uncoupling (CLOU) for combustion of methane. Energy Fuel 23, 5269–5275.
Shulman, A., Cleverstam, E., Mattisson, T., Lyngfelt, A., 2011. Chemical–Looping with oxygen uncoupling using Mn/Mg-based oxygen carriers–Oxygen release and reactivity with methane. Fuel 90, 941–950.
Solunke, R.D., Veser, Gt., 2010. Hydrogen production via chemical looping steam reforming in a periodically operated fixed-bed reactor. Ind. Eng. Chem. Res. 49, 11037–11044.
Son, S.R., Kim, S.D., 2006. Chemical-looping combustion with NiO and Fe_2O_3 in a thermobalance and circulating fluidized bed reactor with double loops. Ind. Eng. Chem. Res. 45, 2689–2696.
Song, H., Shah, K., Doroodchi, E., Wall, T., Moghtaderi, B., 2013. Analysis on chemical reaction kinetics of CuO/SiO2 oxygen carriers for chemical looping air separation. Energy Fuel 28, 173–182.
Song, H., Shah, K., Doroodchi, E., Wall, T., Moghtaderi, B., 2014. Reactivity of Al_2O_3-or SiO_2-Supported Cu-, Mn-, and Co-based oxygen carriers for chemical looping air separation. Energy Fuel 28, 1284–1294.
Song, Q., Xiao, R., Deng, Z., Shen, L., Xiao, J., Zhang, M., 2008a. Effect of temperature on reduction of $CaSO_4$ oxygen carrier in chemical-looping combustion of simulated coal gas in a fluidized bed reactor. Ind. Eng. Chem. Res. 47, 8148–8159.
Song, Q., Xiao, R., Deng, Z., Zhang, H., Shen, L., Xiao, J., Zhang, M., 2008b. Chemical-looping combustion of methane with CaSO4 oxygen carrier in a fixed bed reactor. Energy Convers. Manage. 49, 3178–3187.
Sozinho, T., Pelletant, W., Gauthier, T., Stainton, H., 2012. Main results of the 10 kW coal pilot plant operation. In: 2nd Int. Conf. on Chemical Looping. Darmstadt, Germany. Sep. 26 2012.
Ströhle, J., Orth, M., Epple, B., 2014. Design and operation of a 1 MW_{th} chemical looping plant. Appl. Energy 113, 1490–1495.
Ströhle, J., Orth, M., Epple, B., 2015. Chemical looping combustion of hard coal in a 1 MW_{th} pilot plant using ilmenite as oxygen carrier. Appl. Energy 157, 288–294.
Su, M., Cao, J., Tian, X., Zhang, Y., Zhao, H., 2019. Mechanism and kinetics of Cu_2O oxidation in chemical looping with oxygen uncoupling. Proc. Combust. Inst. 37, 4371–4378.
Su, M., Ma, J., Tian, X., Zhao, H., 2017a. Reduction kinetics of hematite as oxygen carrier in chemical looping combustion. Fuel Process. Technol. 155, 160–167.
Su, M., Zhao, H., Tian, X., Zhang, P., Du, B., Liu, Z., 2017b. Intrinsic reduction kinetics investigation on a hematite oxygen carrier by CO in chemical looping combustion. Energy Fuel 31, 3010–3018.
Su, M., Zhao, H., Ma, J., Zheng, C., 2015a. CFD simulation for chemical looping combustion in dual circulation fluidized bed. J. Combust. Sci. Technol. 21, 363–369 in Chinese.
Su, M., Zhao, H., Ma, J., 2015b. Computational fluid dynamics simulation for chemical looping combustion of coal in a dual circulation fluidized bed. Energ. Convers. Manage. 105, 1–12.
Sun, R., Li, Y., Liu, H., Wu, S., Lu, C., 2012. CO_2 capture performance of calcium-based sorbent doped with manganese salts during calcium looping cycle. Appl. Energy 89, 368–373.
Sun, Z., Wu, X., Russell, C.K., Dyar, M.D., Sklute, E.C., Toan, S., Fan, M., Duan, L., Xiang, W., 2019. Synergistic enhancement of chemical looping-based CO_2 splitting with biomass cascade utilization using cyclic stabilized $Ca_2Fe_2O_5$ aerogel. J. Mater. Chem. A 7, 1216–1226.
Sundqvist, S., Arjmand, M., Mattisson, T., Ryden, M., Lyngfelt, A., 2015. Screening of different manganese ores for chemical-looping combustion (CLC) and chemical-looping with oxygen uncoupling (CLOU). Int. J. Greenh. Gas Con. 43, 179–188.
Tang, M., Xu, L., Fan, M., 2015. Progress in oxygen carrier development of methane-based chemical-looping reforming: a review. Appl. Energy 151, 143–156.
Thon, A., Kramp, M., Hartge, E.-U., Heinrich, S., Werther, J., 2014. Operational experience with a system of coupled fluidized beds for chemical looping combustion of solid fuels using ilmenite as oxygen carrier. Appl. Energy 118, 309–317.
Tian, H., Guo, Q., Yue, X., Liu, Y., 2010. Investigation into sulfur release in reductive decomposition of calcium sulfate oxygen carrier by hydrogen and carbon monoxide. Fuel Process. Technol. 91, 1640–1649.
Tian, X., Dudek, R.B., Gao, Y., Zhao, H., 2019. Redox oxidative cracking of *n*-hexane with Fe-substituted barium hexaaluminates as redox catalysts. Catal. Sci. Technol. 9, 2211–2220.
Tian, X., Niu, P., Ma, Y., Zhao, H., 2018a. Chemical-looping gasification of biomass: part II. Tar yields and distributions. Biomass Bioenergy 108, 178–189.
Tian, X., Wang, K., Zhao, H., Su, M., 2017a. Chemical looping with oxygen uncoupling of high-sulfur coal using copper ore as oxygen carrier. Proc. Combust. Inst. 36, 3381–3388.
Tian, X., Wei, Y., Zhao, H., 2017b. Evaluation of a hierarchically-structured CuO@TiO_2-Al_2O_3 oxygen carrier for chemical looping with oxygen uncoupling. Fuel 209, 402–410.
Tian, X., Wei, Y., Zhao, H., 2018b. Using a hierarchically-structured CuO@TiO_2-Al_2O_3 oxygen carrier for chemical looping air separation in a paralleled fluidized bed reactor. Chem. Eng. J. 334, 611–618.
Tian, X., Zhao, H., Ma, J., 2017c. Cement bonded fine hematite and copper ore particles as oxygen carrier in chemical looping combustion. Appl. Energy 204, 242–253.
Tian, X., Zhao, H., Wang, K., Ma, J., Zheng, C., 2015. Performance of cement decorated copper ore as oxygen carrier in chemical-looping with oxygen uncoupling. Int. J. Greenh. Gas Con. 41, 210–218.
Tong, A., Bayham, S., Kathe, M.V., Zeng, L., Luo, S., Fan, L., 2014. Iron-based syngas chemical looping process and coal-direct chemical looping process development at Ohio State University. Appl. Energy 113, 1836–1845.
Wang, B., Rong, Y., Zheng, Y., Zhao, H., Zheng, C., 2011a. Simulated investigation of chemical looping combustion with coal-derived syngas and $CaSO_4$ oxygen carrier. J. Fuel Chem. Technol. 39, 251–257.
Wang, B., Cao, Y., Li, J., Wang, W., Zhao, H., Zheng, C., 2016a. Migration and redistribution of sulfur species during chemical looping combustion of coal with $CuFe_2O_4$ combined oxygen carrier. Energy Fuel 30, 8499–8510.
Wang, B., Gao, C., Wang, W., Zhao, H., Zheng, C., 2014a. Sulfur evolution in chemical looping combustion of coal with $MnFe_2O_4$ oxygen carrier. J. Environ. Sci. 26, 1062–1070.
Wang, B., Li, J., Ding, N., Mei, D., Zhao, H., Zheng, C., 2017. Chemical looping combustion of a typical lignite with a $CaSO_4$–CuO mixed oxygen carrier. Energy Fuel 31, 13942–13954.
Wang, B., Wang, W., Ma, Q., Lu, J., Zhao, H., Zheng, C., 2016b. In-depth investigation of chemical looping combustion of a Chinese bituminous coal with $CuFe_2O_4$ combined oxygen carrier. Energy Fuel 30, 2285–2294.
Wang, B., Xiao, G., Song, X., Zhao, H., Zheng, C., 2014b. Chemical looping combustion of high-sulfur coal with $NiFe_2O_4$-combined oxygen carrier. J. Therm. Anal. Calorim. 118, 1593–1602.
Wang, B., Yan, R., Lee, D.H., Liang, D.T., Zheng, Y., Zhao, H., Zheng, C., 2008. Thermodynamic investigation of carbon deposition and sulfur evolution in chemical looping combustion with syngas. Energy Fuel 22, 1012–1020.
Wang, B., Yan, R., Lee, D.H., Zheng, Y., Zhao, H., Zheng, C., 2011b. Characterization and evaluation of Fe_2O_3/Al_2O_3 oxygen carrier prepared by sol–gel combustion synthesis. J. Anal. Appl. Pyrol. 91, 105–113.
Wang, B., Yan, R., Zhao, H., Zheng, Y., Liu, Z., Zheng, C., 2011c. Investigation of chemical looping combustion of coal with $CuFe_2O_4$ oxygen carrier. Energy Fuel 25, 3344–3354.
Wang, B., Yan, R., Zheng, Y., Zhao, H., Zheng, C., 2011d. Mechanistic investigation of chemical looping combustion of coal with Fe_2O_3 oxygen carrier. Fuel 90, 2359–2366.
Wang, B., Zhao, H., Zheng, Y., Liu, Z., Yan, R., Zheng, C., 2012a. Chemical looping combustion of a Chinese anthracite with Fe_2O_3-based and CuO-based oxygen carriers. Fuel Process. Technol. 96, 104–115.
Wang, B., Zhao, H., Zheng, Y., Liu, Z., Zheng, C., 2013a. Chemical looping combustion of petroleum coke with $CuFe_2O_4$ as oxygen carrier. Chem. Eng. Tchnol. 36, 1488–1495.
Wang, B., Gao, C., Zhao, H., Zheng, C., 2012b. Preparation of $CoFe_2O_4$ nanocrystallite by sol-gel combustion synthesis and evaluation of its reaction performance. Adv. Mater. Res. 341, 63–67.
Wang, C., Ma, J., Zhao, H., Tian, X., 2018. Systematic investigation on sulfur behavior in coal-derived in situ gasification chemcial looping combustion process. In: 5th International Conference on Chemical Looping. Utah, USA, Sep. pp. 24.
Wang, J., Zhao, H., 2015. Chemical looping dechlorination through adsorbent-decorated Fe_2O_3/Al_2O_3 oxygen carriers. Combust. Flame 162, 3503–3515.
Wang, J., Zhao, H., 2016. Application of CaO-decorated iron ore for inhibiting chlorobenzene during in situ gasification chemical looping combustion of plastic waste. Energy Fuel 30, 5999–6008.
Wang, K., Tian, X., Zhao, H., 2016c. Sulfur behavior in chemical-looping combustion using a copper ore oxygen carrier. Appl. Energy 166, 84–95.
Wang, K., Yu, Q., Qin, Q., 2013b. Reduction kinetics of Cu-based oxygen carriers for chemical looping air separation. Energy Fuel 27, 5466–5474.
Wang, K., Yu, Q., Qin, Q., Zuo, Z., Wu, T., 2016d. Evaluation of Cu-based oxygen carrier for chemical looping air separation in a fixed-bed reactor. Chem. Eng. J. 287, 292–301.
Wang, K., Zhao, H., Tian, X., Fang, Y., Ma, J., Zheng, C., 2015. Chemical-looping with oxygen uncoupling of different coals using copper ore as an oxygen carrier. Energy

Fuel 29, 6625–6635.
Wang, Y., Niu, P., Zhao, H., 2019. Chemical looping gasification of coal using calcium ferrites as oxygen carrier. Fuel Process. Technol. 192, 75–86.
Wei, G., He, F., Huang, Z., Zheng, A., Zhao, K., Li, H., 2015. Continuous operation of a 10 kW_{th} chemical looping integrated fluidized bed reactor for gasifying biomass using an iron-based oxygen carrier. Energy Fuel 29, 233–241.
Wen, Y., Li, Z., Xu, L., Cai, N., 2012. Experimental study of natural Cu ore particles as oxygen carriers in chemical looping with oxygen uncoupling (CLOU). Energy Fuel 26, 3919–3927.
Xiao, R., Song, Q., Song, M., Lu, Z., Zhang, S., Shen, L., 2010. Pressurized chemical-looping combustion of coal with an iron ore-based oxygen carrier. Combust. Flame 157, 1140–1153.
Xu, H., Ma, J., Zhao, H., 2018. Macroscopic fuel reactor modelling of a 5 kW_{th} interconnected fluidized bed for in-situ gasification chemical looping combustion of coal. Chem. Eng. J. 348, 978–991.
Xu, L., Sun, H., Li, Z., Cai, N., 2016. Experimental study of copper modified manganese ores as oxygen carriers in a dual fluidized bed reactor. Appl. Energy 162, 940–947.
Xu, L., Wang, J., Li, Z., Cai, N., 2013. Experimental study of cement-supported CuO oxygen carriers in chemical looping with oxygen uncoupling (CLOU). Energ. Fuel 27, 1522–1530.
Xu, Z., Zhao, H., Wei, Y., Zheng, C., 2015. Self-assembly template combustion synthesis of a core–shell $CuO@TiO_2$–Al_2O_3 hierarchical structure as an oxygen carrier for the chemical-looping processes. Combust. Flame 162, 3030–3045.
Xu, Z., Zhao, H., Zhao, H., 2017. CFD-population balance Monte Carlo simulation and numerical optimization for flame synthesis of TiO_2 nanoparticles. Proc. Combust. Inst. 36, 1099–1108.
Yang, W., Zhao, H., Ma, J., Mei, D., Zheng, C., 2014. Copper-decorated hematite as an oxygen carrier for in situ gasification chemical looping combustion of coal. Energy Fuel 28, 3970–3981.
Yang, W., Zhao, H., Wang, K., Zheng, C., 2015. Synergistic effects of mixtures of iron ores and copper ores as oxygen carriers in chemical-looping combustion. Proc. Combust. Inst. 35, 2811–2818.
Yusuf, S., Neal, L.M., Li, F., 2017. Effect of promoters on manganese-containing mixed metal oxides for oxidative dehydrogenation of ethane via a cyclic redox scheme. ACS Catal. 7, 5163–5173.
Zafar, Q., Abad, A., Mattisson, T., Gevert, B., Strand, M., 2007. Reduction and oxidation kinetics of Mn_3O_4/Mg–ZrO_2 oxygen carrier particles for chemical-looping combustion. Chem. Eng. Sci. 62, 6556–6567.
Zeng, L., Cheng, Z., Fan, J.A., Fan, L., Gong, J., 2018. Metal oxide redox chemistry for chemical looping processes. Nat. Rev. Chem. 2, 349–364.
Zhang, J., Haribal, V., Li, F., 2017. Perovskite nanocomposites as effective CO_2-splitting agents in a cyclic redox scheme. Sci. Adv. 3, e1701184.
Zhang, T., Li, Z., Cai, N., 2009. Continuous O_2-CO_2 production using a Co-based oxygen carrier in two parallel fixed-bed reactors. Korean J. Chem. Eng. 26, 845–849.
Zhang, Y., Zhao, H., Guo, L., Zheng, C., 2015. Decomposition mechanisms of Cu-based oxygen carriers for chemical looping with oxygen uncoupling based on density functional theory calculations. Combust. Flame 162, 1265–1274.
Zhao, H., Liu, L., Di, X., Zheng, C., Liu, G., Jiangt, L., 2008a. $NiO/NiAl_2O_4$ oxygen carriers prepared by sol-gel for chemical-looping combustion fueled by gas. J. Fuel Chem. Technol. 36, 261–266.
Zhao, H., Gui, J., Cao, J., Zheng, C., 2018. Molecular dynamics simulation of the microscopic sintering process of CuO nanograins inside an oxygen carrier particle. J. Phys. Chem. C 122, 25595–25605.
Zhao, H., Guo, L., Zou, X., 2015. Chemical-looping auto-thermal reforming of biomass using Cu-based oxygen carrier. Appl. Energy 157, 408–415.
Zhao, H., Liu, L., Wang, B., Xu, D., Jiang, L., Zheng, C., 2008b. Sol–gel-derived $NiO/NiAl_2O_4$ oxygen carriers for chemical-looping combustion by coal char. Energy Fuel 22, 898–905.
Zhao, H., Mei, D., Ma, J., Zheng, C., 2014a. Comparison of preparation methods for iron–alumina oxygen carrier and its reduction kinetics with hydrogen in chemical looping combustion. Asia-Pac. J. Chem. Eng. 9, 610–622.
Zhao, H., Wang, J., 2018. Chemical-looping combustion of plastic wastes for in situ inhibition of dioxins. Combust. Flame 191, 9–18.
Zhao, H., Wang, K., Fang, Y., Ma, J., Mei, D., Zheng, C., 2014b. Characterization of natural copper ore as oxygen carrier in chemical-looping with oxygen uncoupling of anthracite. Int. J. Greenh. Gas Con. 22, 154–164.
Zhao, H., Xu, Z., Zhao, H., 2019. Population balance monte carlo simulation of self-assembly of core (micro-Al_2O_3)-shell (nano-TiO_2) structure in aqueous suspensions. Chem. Eng. Sci. 199, 100–112.
Zhao, H., Zhang, Y., Wei, Y., Gui, J., 2017. Understanding CuO-support interaction in Cu-based oxygen carriers at a microcosmic level. Proc. Combust. Inst. 36, 4069–4077.
Zhao, Z., Chen, T., Ghoniem, A.F., 2012a. Rotary bed reactor for chemical-looping combustion with carbon capture. Part 1: reactor design and model development. Energy Fuel 27, 327–343.
Zhao, Z., Chen, T., Ghoniem, A.F., 2012b. Rotary bed reactor for chemical-looping combustion with carbon capture. Part 2: base case and sensitivity analysis. Energy Fuel 27, 344–359.
Zheng, M., Shen, L., Xiao, J., 2010. Reduction of CaSO4 oxygen carrier with coal in chemical-looping combustion: effects of temperature and gasification intermediate. Int. J. Greenh. Gas Con. 4, 716–728.
Zheng, Y., Li, K., Wang, H., Tian, D., Wang, Y., Zhu, X., Wei, Y., Zheng, M., Luo, Y., 2017. Designed oxygen carriers from macroporous $LaFeO_3$ supported CeO_2 for chemical-looping reforming of methane. Appl. Catal. B-Environ. 202, 51–63.
Zhou, Z., Han, L., Nordness, O., Bollas, G.M., 2015. Continuous regime of chemical-looping combustion (CLC) and chemical-looping with oxygen uncoupling (CLOU) reactivity of CuO oxygen carriers. Appl. Catal. B-Environ. 166, 132–144.
Zhu, X., Li, K., Neal, L., Li, F., 2018a. Perovskites as geo-inspired oxygen storage materials for chemical looping and three-way catalysis: a perspective. ACS Catal. 8, 8213–8236.
Zhu, X., Li, K., Wei, Y., Wang, H., Sun, L., 2014. Chemical-looping steam methane reforming over a CeO_2–Fe_2O_3 oxygen carrier: evolution of its structure and reducibility. Energy Fuel 28, 754–760.
Zhu, X., Zhang, M., Li, K., Wei, Y., Zheng, Y., Hu, J., Wang, H., 2018b. Chemical-looping water splitting over ceria-modified iron oxide: performance evolution and element migration during redox cycling. Chem. Eng. Sci. 179, 92–103.